Design and Validation of Batch Crystallizer to Study Non-Photochemical Laser-Induced Nucleation

Ishtyaque Ahmed Ansari

Technische Universiteit Delft

TU Delft Delft University of Technology

Challenge the future

Design and Validation of Batch Crystallizer to Study Non-Photochemical Laser-Induced Nucleation

by

Ishtyaque Ahmed Ansari

in partial fulfillment of the requirements for the degree of

Master of Science
in Chemical Engineering

at the Delft University of Technology,
to be defended publicly on 26th May 2021 at 02.00 PM

Student number:	5076358	
Thesis committee:	Dr. H. B. Eral,	TU Delft, supervisor
	Prof.dr. A.E.D.M. van der Heijden,	TU Delft
	Dr. Bijoy Bera,	TU Delft
Daily supervisor:	Dr. Frederico Marques Penha,	KTH Royal Institute of Technology
	Vikram B. Korede,	TU Delft

An electronic version of this thesis is available at http://repository.tudelft.nl/.
Front cover image is the microscopic image of potassium chloride

TU Delft Delft University of Technology

Abstract

Crystallization is an important process occurring in nature, pharmaceutical, and food industries. It is one of many widely used unit operations for the separation and purification of chemicals industrially. Despite its far-reaching application in fine chemicals and active pharmaceutical ingredients production, the stochastic nature of nucleation makes it difficult to obtain crystals with reproducible properties like size, structure, purity, and polymorphic form. The accidental discovery of Non-Photochemical Laser-Induced Nucleation (NPLIN) in 1996 emerged as a novel technique to tame the crystallization process. Since the laser provided better spatiotemporal control over crystal properties in a solution, NPLIN gained abundant traction over past decades in the vial and microfluidic scaled experiments.

On the contrary, this research studies the NPLIN effect in potassium chloride (KCl) solution on a liter scale. A batch cooling crystallizer coupled with an irradiation source in the form of the laser beam is investigated here as proof of the concept study. NPLIN experiments were conducted in batch crystallizer and were compared with the control experiments. Interestingly, the laser source reduced the induction time of nucleation compared to control experiments. This phenomenon showed that the nucleation kinetics can be controlled using laser properties. Furthermore, it was observed experimentally that the nuclei generated by laser in an undersaturated solution can be grown to a detectable size provided the supersaturation is increased. It was also observed that the crystal number density was more with the multiple pulses as compared to a single pulse owing to the large exposed volume by irradiation of multiple pulses in agitated bulk solution. Finally, the offline particle size distribution (PSD) comparison was done. The dominant size of crystals was 100-200 μm for the control experiment whereas, it was 300-500 μm for the NPLIN experiment. It revealed a clear shift in the peak of the dominant size of crystals indicating a growth dominant event in NPLIN experiments. Appealingly, the nature of PSD generated by laser irradiation was found similar in all repetitions. It is hypothesized that the laser generates the seeds which grow in the metastable region.

This research study provides the basis for the NPLIN study in the system resembling industrial conditions. This, in turn, will aid in the understanding of the nucleation process and, ultimately, the optimization of industrial crystallization. The results obtained can also be used to develop mathematical models for particle size distribution.

Acknowledgements

This project gave me an excellent opportunity to explore the realm of crystallization and helps to attain the skill-set required in the scientific world. Apart from learning about conventional chemical engineering equipment like batch cooling crystallizer, I am more amazed to learn about laser and optics. This project is perfect blend of interdisciplinary research areas and I really enjoyed the process of learning through this project. The journey of this project had its own crests and troughs which would have not been successful without the valuable support of many people.

First of all I would bow down my head to the omnipresent and omniscient Almighty, as a result of his clemency my project was fully consummated. I feel emotionally moved when it comes to acknowledgment after the task is completed. I thank one and all, first of all my loving and caring family, supervisor, mentors, friends and elders who have contributed alot during my project.

It is my ardent task to record my debt to my supervisor Dr. Burak Eral for giving me the platinum opportunity to work on this project. His invaluable guidance, whole hearted support and encouragement through weekly group meetings helped me to accomplish the project in a fruitful direction. It has been an absolute honour to co-work with my daily supervisors, Fred and Vikram for their dynamism, fantastic stamina and day to day monitoring were a constant source of inspiration for me.

I specially appreciate the help extended by Dr. D. Irimia for training and guiding me to perform NPLIN experiment along with operating the laser. I also thank Ajinkya Pandit for discussions and guiding me in this project. Special thanks to Roshan, Ratul, Nazia, Khushboo, Avinash, Meet, Gaurav and all my friends for their persistent moral support, motivation at times when the globe is facing pandemic.

I hope you will really enjoy reading my research report.

Ishtyaque Ahmed Ansari
Delft, May 2020

Contents

List of Figures

List of Tables

Abbreviations

CWR	Cooling water return
CWS	Cooling water supply
FBRM	Focused beam reflectance measurement
GUI	Graphic user interface
LED	Light emitting diode
NPLIN	Non-photochemical laser-induced nucleation
PSD	Particle size distribution
SOPAT	Smart online particle analysis technology
TNT	Two step nucleation theory

1

Introduction

"I am among those who think that science has great beauty."

– Marie Curie

1.1. Motivation

Crystallization is one of the vital separation techniques used in the process industry. A plethora of chemicals can be produced by this technique industrially[1]. Du Pont, one of the largest chemical manufacturers estimated in 1988 that around 70% of the product involves crystallization process[2]. The crystallization process is also used as separation and purification techniques in pharmaceutical industries. In 2017, it was estimated that the total worldwide pharmaceutical market value at ex-factory prices was around 208.95 Billion Euro and the dutch pharmaceutical production was around 6.18 Billion Euro[3]. From these statistics, it is evident that crystallization holds a large economical share.

Crystallization can be defined as the phase change process in which crystalline product is separated from the solution. The crystallization phenomenon comprises two steps: nucleation and growth[4]. However, the working mechanism of nucleation is still not fully comprehended[5]. This can be attributed to the size and time scales that make it difficult to observe it[6]. This makes it difficult to obtain reproducible crystal properties industrially. Hence, a comprehensive understanding of the crystallization process at the fundamental and molecular level is required for the improvement of industrial crystallization. This in turn will help to achieve better control over crystal purity, size, shape, and polymorphism, also known as the four pillars of crystal engineering.

The driving force for crystallization is supersaturation. Based on this, there are different crystallization techniques used industrially. In these techniques, the supersaturation is increased in a controlled manner. It can be achieved by slow cooling of solute known as cooling crystallization, evaporation of the solvent known as evaporative crystallization, or by addition of antisolvent to the solution. However, the control over crystal properties is very less by using these techniques[7]. Therefore, novel experimental techniques are developed such as sonocrystallization[8], microwave-assisted crystallization[9], and non-photochemical induced nucleation (NPLIN)[5]. This report focuses on the understanding of NPLIN.

NPLIN is the physiochemical phenomenon in which a light source such as an intense nanosecond laser pulse induces nucleation in a relatively lower supersaturated solution that usually takes a longer time to nucleate. It was first observed by Garetz et al. in 1996 in an attempt to observe the second harmonic generation in supersaturated aqueous urea solution[10]. After some time of laser irradiation, needle-shaped crystals aligned with the laser electric field were observed without affecting the chemical composition. It emerged as a novel technique to tame the crystallization process. It influences the nucleation energy barrier at the molecular level, unlike the classical crystallization mechanisms that rely on overall supersaturation. In literature, there are various possible mechanisms like optical Kerr effect, dielectric polarization, and nano-particle heating[10–12]. But, these proposed mechanisms are inconsistent and cannot explain

the nucleation completely. Due to the debatable proposed mechanisms, it is a challenging task to implement it on industrial scale. Moreover, it has also been observed that the laser properties like intensity, pulse duration, and the number of pulses influence the crystal characteristics[13]. Due to this, it opens a new domain of research to tame the crystallization by using NPLIN.

1.2. RESEARCH GOALS

The goal of this project is to build a proof of concept of batch cooling crystallizer coupled with an irradiation source in the form of a laser beam to understand NPLIN in a liter scale volume. The developed batch cooling crystallizer setup will be used to conduct control experiments and compare laser-induced nucleation experiments to control experiments. Additionally, the onset of nucleation will be recorded with inline instruments: FBRM (Focused Beam Reflectance Measurement), and SOPAT (Smart Online Particle Analysis Techniques). This thesis work is dedicated to the development of an innovative laser-assisted prototype that aims at providing temporal and spatial control of crystals in flow reactors.

A batch cooling crystallizer is used for the initial proof of concept. The experimental conditions resemble quite closely industrial conditions and most importantly it has a mixing condition similar to the previous one. In this project, conventional cooling crystallization is studied with recently developed NPLIN experiments. This will provide better insight to understand the behaviour of light source on the conventional batch cooling experiments. NPLIN is dedicated to studying the stochastic nature of nucleation, so this setup will help to understand the nucleation mechanism in industrial processes with better control of crystal size, polymorphism, and number density.

1.3. THESIS OUTLINE

This project starts with a literature review and subsequent chapters follow a chronological order: solubility studies of aqueous potassium chloride and its dependency on temperature, the development of setup with control experiments of cooling crystallization, laser experiments on the batch crystallizer to study the effect on induction time, and particle size distribution. Each chapter is further divided into various sub-sections with theory, equipment description, materials and methods along with necessary results and discussion.

2

Theory & Literature Review

"Everything is theoretically impossible, until it is done."

– Robert A. Heinlein

2.1. Introduction

This chapter entails the background of crystallization, the nucleation mechanism, and the factors affecting the nucleation. Additionally, it also provides information about the conventional batch cooling crystallization and the Non-Photochemical Laser-Induced Nucleation (NPLIN). This chapter builds the theoretical context for various terminologies and concepts that are used in the development of the research work.

2.2. Crystallization

Crystallization is a phase change process in which the randomly organized solute molecules in fluid come together to form an ordered three-dimensional crystal structure[4]. This phenomenon occurs in two main steps. The first step is nucleation in which the cluster of solute particles come together to form a nucleus. Subsequently, the growth of this nucleus takes place as an independent unit in an orderly well defined molecular arrangement know as crystal lattice as shown in Figure 2.1[14]. The unpredictability of cluster size and structure makes this process stochastic. The initial orientation and structure at the onset of nucleation also determine the final crystal arrangement[4].

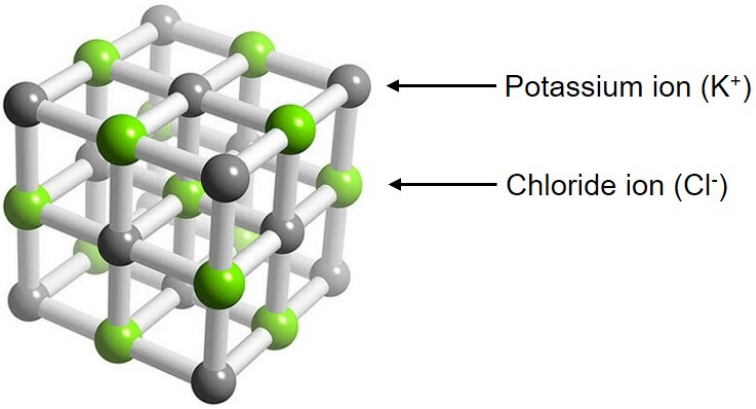

Figure 2.1: Crystal lattice structure of KCl [15]

2.3. NUCLEATION MECHANISM

Crystallization starts with the birth of a crystal in the nucleation phase. The fundamental driving force for crystallization is the chemical potential difference between the given solute in the solution and the generated crystal. After assuming the solution to be an ideal solution, the relation between the chemical potential and supersaturation is given by Equation 2.1, where $\Delta\mu$ is the chemical potential difference, R is the universal gas constant, T is absolute temperature, a is the activity of solute, and a^* is the activity of solute at equilibrium[16].

$$\frac{\Delta\mu}{RT} = \ln\left(a/a^*\right) = \ln S. \tag{2.1}$$

Ideally, there exists a maximum amount of solute that can dissolve in a solvent at a given temperature. This is known as the saturation limit. If there is more solute than the saturation limit, it is known as a supersaturation solution. Whereas, if the solute is less than the saturation limit, it is known as an undersaturation solution. The supersaturation (S) is defined as the ratio of the solute concentration to the solute solubility at that temperature. It is given by Equation 2.2 where C is the solute concentration and C^* is the solute solubility at a given temperature. The supersaturation of a compound can be varied by changing the temperature. The relationship between the solubility and the temperature is given by the solubility diagram as shown in Figure 2.2.

$$S = \frac{C}{C^*}. \tag{2.2}$$

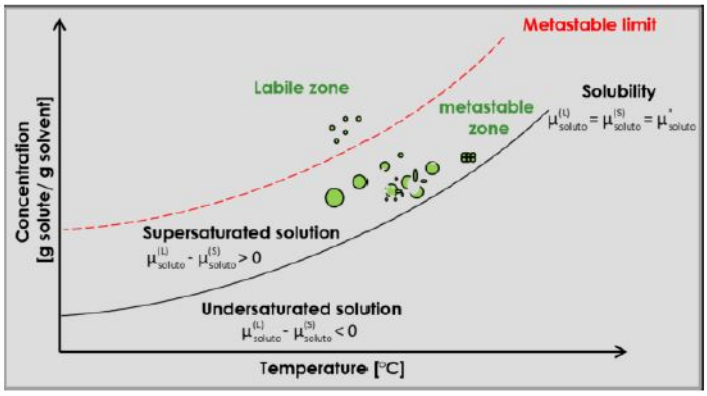

Figure 2.2: Solubility curve with metastable zone width. Image taken from[17].

Figure 2.2 is classified into three regions based on the likelihood of a solution undergoing nucleation. These are undersaturated, metastable, and labile zone. The stable zone is bounded by the equilibrium line and the solution remains always in undersaturated condition. The metastable and labile zone corresponds to the supersaturated region. In the metastable zone, no spontaneous nucleation takes place wherein labile zone, spontaneous uncontrolled nucleation takes place. There is no clear boundary line exists between these two zones. The boundary line mentioned here depends on various factors such as heating and cooling rates or the volume of the solution[18]. To understand the crystallization more effectively, a better grasp of nucleation and crystal growth is necessary.

The basic apprehension of the nucleation mechanism can be done by classifying it into broader groups which are shown in Figure 2.3.

Primary nucleation takes place spontaneously in the bulk of liquid where no pre-existing nucleus is present. It is further classified into two groups: homogeneous and heterogeneous nucleation. Homogeneous nucleation refers to nuclei formation in the absence of any crystalline surface. It is very difficult to observe homogeneous nucleation due to the unavoidable presence of crystalline surfaces such as impurities, crystallizer walls, or stirrer. These nanoparticle impurities can also enter into the system either through sample preparation or already present in the sample. Contrarily, the heterogeneous nucleation takes place in presence of foreign particles like dust or impurities that are present in the solution. These foreign particles act as active

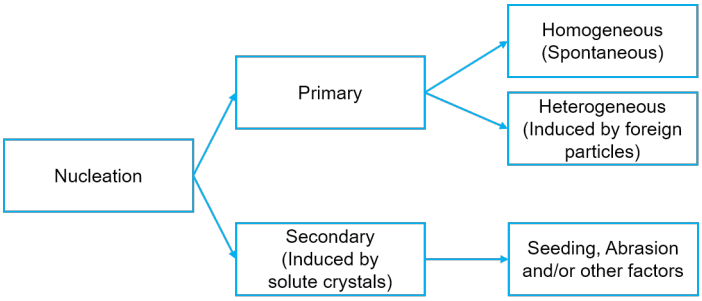

Figure 2.3: Classification of nucleation types[16]

sites increasing locally the probability of nucleation as compared to other sites in bulk liquid[19].

Secondary nucleation takes place in the presence of pre-existing crystals known as seeds. These seeds act as catalysts for nucleation. As shown in Figure 2.4 the secondary nucleation takes place either on the surface of the seeds, the interaction of crystal with each other or with the surface of the crystallizer, or the particles formed by the breakage of fully grown crystals[4].

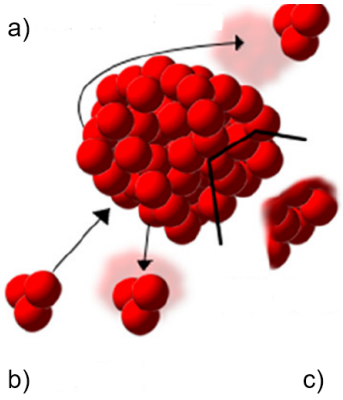

Figure 2.4: Secondary nucleation due to (a) shear force applied by fluid layer, (b) impact from other crystal particle or impeller, and (c) breakage of crystals due to mechanical impact. Image taken from literature[20].

There are two theories available in the literature explaining the nucleation mechanism: Classical nucleation theory, and Two-step nucleation theory.

2.3.1. CLASSICAL NUCLEATION THEORY

Classical nucleation theory (CNT) is the oldest and widely used nucleation mechanism to explain homogeneous nucleation. It was originally developed by Volmer and Weber in 1913[21] to explain the condensation of the vapor phase into the liquid but it can also be used as an analogy to explain the crystallization. At the end of the 19th century, the thermodynamic description of CNT was given by Gibbs[14]. He defined the total free energy required for the cluster formation (ΔG) as the algebraic sum of volume free energy change (ΔG_v) when solute precipitates as crystals, and the surface free energy change (ΔG_s) due to interface formed between crystal and bulk liquid.

$$\Delta G = \Delta G_v + \Delta G_s. \tag{2.3}$$

In Equation 2.3, the first term favors the nucleation of crystals. This is because the solid state is thermodynamically more stable than the liquid state. Contrarily, the second surface term becomes positive proportionally to the surface formed due to crystal formation, hence favours the dissolution of the generated nucleus. Therefore, the total free energy (ΔG) is the final result of these two competing factors. As it can be seen in Figure 2.5, the total free energy reaches a maximum (ΔG^*) at critical radius (r^*), after which total

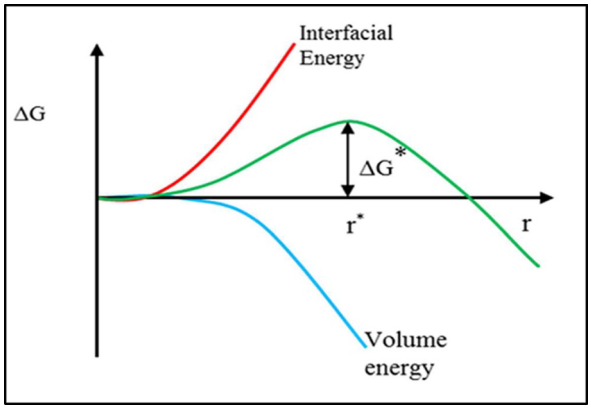

Figure 2.5: Free energy barrier in classical nucleation theory. Image taken from literature[22]

free energy decreases with an increase in cluster radius (r). The minimum energy needed for the clusters to grow is given by Equation 2.4

$$\Delta G^* = \frac{4\pi\sigma r^{*2}}{3}. \tag{2.4}$$

This theory is based on the assumption that all nuclei clusters are spherical and the interaction between clusters, or pre-existing nuclei is ignored. All clusters grow into an orderly molecular arrangement called a crystal lattice. This makes the theory analytically simple to apply. The steady-state nucleation rate (J) i.e., the number of crystals formed per unit volume per unit time according to CNT is given by Equation 2.5[21].

$$J = A\exp\left(\frac{-\Delta G^*}{k_B T}\right), \tag{2.5}$$

where k_B is Boltzmann's constant and A is pre-exponential factor. However, this theory does not provide details about the path followed by prenucleation clusters to develop into a fully grown crystal.

2.3.2. TWO-STEP NUCLEATION THEORY (TST)

This theory was proposed initially to explain the crystallization in short-range interacting molecules like protein and globular molecules in solution[14]. It assumes that the clusters of solute molecules have to overcome two energy barriers: first amorphous high dense liquid-like clusters are formed due to density fluctuations and then molecular rearrangements take place to orderly arranged stable nucleus[14]. The main difference between CNT and TST is explained via Figure 2.6 showing the routes of crystal formation. The later step of rearrangement in TST is proposed to be the rate-determining step thus explaining why complex molecules take a longer time to crystallize[14].

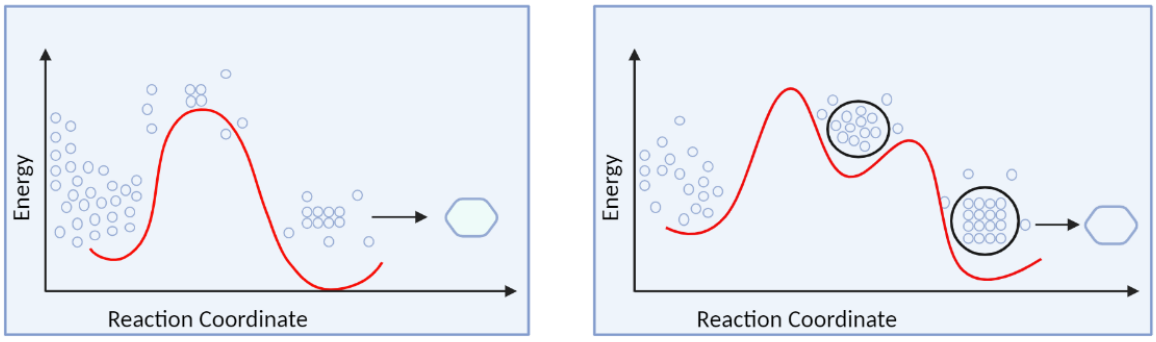

Figure 2.6: Different pathways in Classical nucleation theory(left), and Two-step nucleation theory(right). Image taken from literature[23].

2.4. BATCH COOLING CRYSTALLIZATION

The batch crystallizers are widely used in pharmaceutical and fine specialty chemicals manufacturing industries where the crystalline product is obtained at the end of each batch cycle. It is relatively simple in operation and requires less maintenance. In this, the cooling is done via heat exchange between the bulk solution and the coolant fluid. The driving force for crystallization is supersaturation. The desired supersaturation is achieved by decreasing the temperature at a particular cooling rate. The crystalline product is obtained upon reaching desired supersaturation. This process is mainly used for systems with steep solubility curve[4].

In batch cooling crystallization, the control of final crystal size distribution, crystal purity, and morphology is challenging due to the complexity and non-linearity of the process[24]. It is, therefore, very important to control the various process parameters as explained in this section.

- **Agitation rate**
  The mechanical disturbances always facilitate the nucleation event, however, the agitation rate is not always proportional to nucleation rate due to complex relationships between them[25]. In batch crystallizer, the agitation is mainly done by an impeller. The type of impeller used plays a huge role in both the mixing and secondary nuclei generation. At a low stirring rate, the mixing will be non-uniform, and only very few nucleated crystals will be exposed to different hydrodynamic conditions. Due to this, particular size grown crystals will settle to the bottom of the vessel and the growth rate will be decreased[24]. At a high stirring rate, all nucleated crystals will expose to favorable hydrodynamic conditions required for mass transfer, and hence all crystals are bigger with regular shape[24]. Thus, the stirring governs the hydrodynamic condition inside the crystallizer which in turn has a large effect on the metastable zone width. However, a higher stirrer rate also promotes the secondary nucleation due to breakage of grown crystals by shear force of impeller[26]. Therefore, an optimum stirring speed needs to be maintained to avoid the breakage of crystals with favorable hydrodynamic conditions for mass transfer.

- **Cooling profile**
  The supersaturation can be controlled by manipulating the temperature of the solution. The supersaturation quantifies the excess solute present in the bulk solution. At high supersaturation, the tendency of crystallization is more and once nucleated, it will grow in a specific molecular orientation until the bulk solution reaches saturation level at that temperature. Since the supersaturation is the driving force for the crystallization so the cooling profile predominantly governs the nucleation kinetics. At a fast cooling rate, higher supersaturation is achieved very soon which results in a higher nucleation rate with a large number of crystals with smaller size[24]. The nucleation rate and growth rate compete with each other to consume the supersaturation provided if supersaturation is continuously being generated. If the cooling rate is slow then supersaturation is maintained for a longer time which will facilitate the growth of crystals[24]. Noteworthy here is that 'fast' and 'slow' cooling rates, and supersaturation rates are relative to each system.
  The cooling profile largely affects the final particle size distribution (PSD) of crystals. For example, the linear cooling profile generates the broader PSD of crystals with a smaller mean size[4]. Additionally, the model-based optimum cooling strategy is also developed to achieve narrower PSD with a large mean size of crystals[27, 28].

- **Impurities**
  The nucleation probability increases significantly with the presence of impurities in the bulk solution. As described in the previous section, it induces heterogeneous nucleation by providing an extra surface. These impurities can be dirt/dust present in the environment or they can come from the vessel wall. If the stirrer is not chosen wisely then impurities can come in the form of small particles sheared off from the stirrer. Impurities can also enter into the system while sample preparation or can already be present as chemical impurities in solute and solvent. These impurities can affect the nucleation kinetics, the growth rate, habit, and crystal morphology[29].

2.5. NPLIN

Non-Photochemical Laser-Induced Nucleation (NPLIN) was discovered by Garetz et al.[10] while studying the laser properties in a supersaturated solution of urea. It was observed that Q-switched Nd:YAG nanosecond pulsed laser can induce nucleation and reduces drastically the time required for crystallization at particular supersaturation. The alignment of the crystals was also controlled by the polarization of the light[10].

NPLIN is one of the novel methods to enhance the control over crystal properties in industrial processes. NPLIN experiments were successfully conducted on various inorganic and organic chemicals like KCl, sulfathiazole, glycine, L-histidine, hen egg white protein in solvents like water, ethanol, and agarose gel[30–34]. The term 'Non-Photochemical' is used because the laser beam does not change the chemical properties of the solution[35]. NPLIN provides a high degree of temporal and spatial control in crystallization, as compared to other nucleation methods. It has a certain experimental intensity range as shown in Figure 2.7. Hence, the first recommended step is finding out this experimental range before developing any experimental setup for NPLIN experiments.

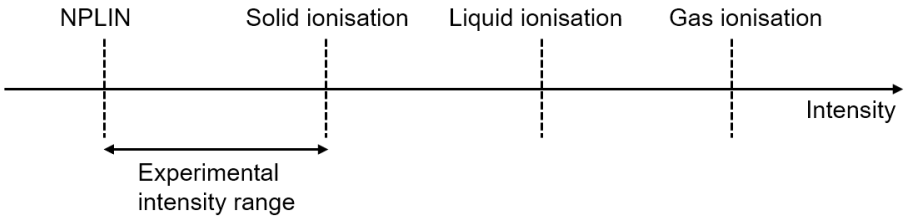

Figure 2.7: Observed thresholds for NPLIN, and solid, liquid and gas ionization. Image taken from literature[36].

2.5.1. THEORY BEHIND NPLIN

Despite the vast experimental evidence of NPLIN on various systems, no consensus has been achieved on its main governing mechanism. The subsections further illustrate the various proposed mechanisms mentioned in the literature.

2.5.1.1. OPTICAL-KERR EFFECT (OKE)

Garetz et al.[10] first proposed this mechanism to explain the formation of needle-shaped crystals in the NPLIN experiment of supersaturated urea solution. It was hypothesized that the oscillating electric field of the incident beam induces a dipole moment in solute molecules which aligns the anisotropic polarization axis of the randomly organized cluster into the direction of the incident beam. This facilitates the pre-clusters into a more organized molecular arrangement and aids the formation of crystals as shown in Figure 2.9. This hypothesis was further used to explain the formation of different polymorphs or crystal structures depending on the polarization of the incident beam, known as 'Polarization Switching'[30], where a linearly polarized incident beam can induce γ form of glycine whereas a circularly polarized incident beam can induce α form of glycine in supersaturated solution[37]. Similar polarization switching in aqueous solution of l-histidine was also reported[31]. However, this hypothesis fails to explain the mechanism behind NPLIN in carbonated water and halides and raising doubt on its validity[38]. It was also reported that the interaction energy between the incident electric field and induced dipole is much lower than the laser intensity used[37]. Hence, the torque applied on solute molecules will be insufficient to reduce the energy barrier. Knott et al. [39] did Monte Carlo simulation to study OKE and concluded that the experimental electric field strengths will be insufficient to reduce the energy barrier required for nucleation.

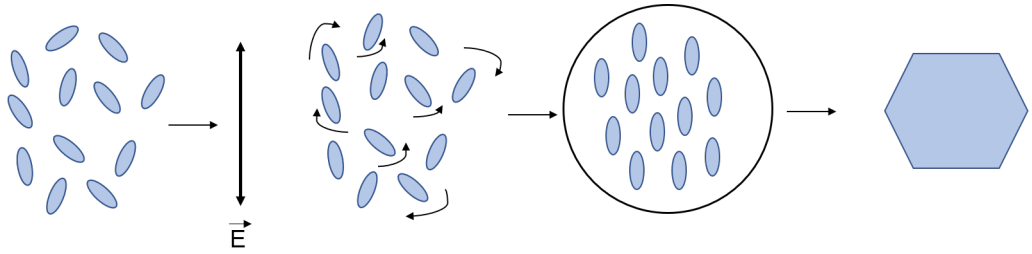

Figure 2.8: Schematics of OKE hypothesis in which laser electric field induces dipole in prenucleating clusters resulting into alignment of clusters in the laser electric field direction leading to crystal formation. Image adapted from literature[23].

2.5.1.2. Isotropic Electronic Polarization

The OKE model fails to explain the cubical shape of KCl crystals which lacks the preferential polarization axis. So, a new mechanism of isotropic electronic polarization was proposed by Alexander et al. while performing NPLIN experiments with KCl at laser peak intensities much lower than Garetz et al[33]. The electric polarization of atoms refers to the shift of the electronic clouds towards the positively charged clusters. The incidence of the laser pulse on solution makes the electric field of the laser polarize the subcritical clusters of the nuclei resulting in the decrease of its free energy barrier. Mathematically, the free energy barrier is proportional to -(ϵ_p-ϵ_s) E^2 where ϵ_p, ϵ_s are dielectric permittivity of solute and solvent respectively and E is the applied electric field. The cluster formed will be stable as long as $\epsilon_p > \epsilon_s$[11]. This reduction in energy barrier leads to the formation of a stable cluster slightly lower than the critical radius and development into the macroscopic crystal as explained in Figure 2.9. This theory explains the nucleation mechanism in most alkali halides but failed to explain the phenomenon on other systems, e.g. carbonated water, as well as the polarization switching[5].

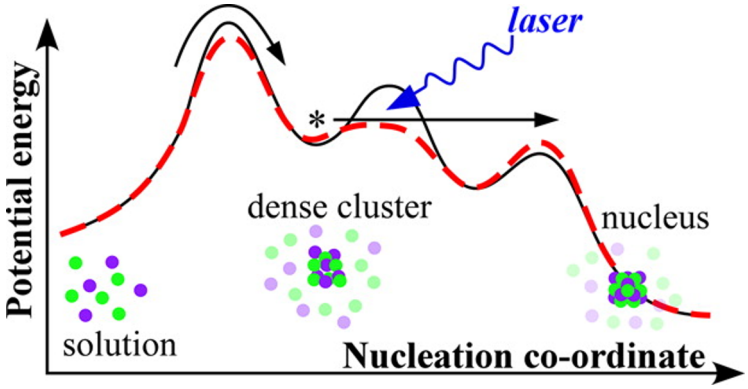

Figure 2.9: Reduction in energy barrier of prenucleating crystals due to dielectric polarization as suggested by Ward et al. [40].

2.5.1.3. Nano-Particle heating

There are some impurities always present in the experimental sample either in the form of molecular impurities (intrinsic) or dust particles (extrinsic). These nanoparticles/nanoimpurities can be heated up by absorbing the energy from the irradiated laser pulse in the solution. The absorbed energy is further transferred adiabatically to the surrounding liquid to vaporize the liquid around particles resulting in a vapour bubble. It has been proposed that the growth of vapour bubbles leads to the accumulation of solute molecules on to the vapour-liquid interface and, hence inducing nucleation. However, recording visual evidence for this mechanism is very challenging due to the inaccessible spatial and temporal scales. The experiments supporting this mechanism were observed by Martin et al. in laser-induced nucleation of NH_4Cl where the main impurities in solute were iron and phosphate. It was observed that the nucleation probability decreased when the impurities were removed via filtration[41]. Kacker et al.[13] also reported a similar observation of low nucleation probability in the filtered sample. This hypothesis is further supported with the

experimental and modeling results showing the increase in temperature of nanoparticles (around 1000-2200K)[42, 43].

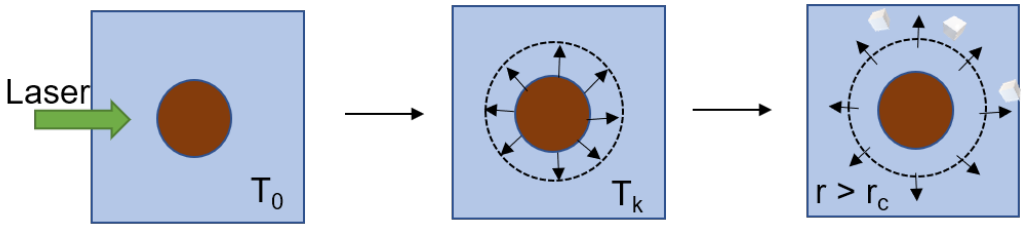

Figure 2.10: Schematic of nano-particle heating hypothesis. Laser heats the nano-particle/dirt which forms cavitation bubble around it and induce nucleation due to local increase in supersaturation. Image taken from literature[5].

2.5.2. FACTORS AFFECTING NPLIN

The nucleation event in the NPLIN experiment is highly stochastic in nature. Since its discovery in 1996, various parameters affecting NPLIN are investigated which is summarized in the following subsection.

- **Laser intensity**
  NPLIN is highly influenced by the peak power laser intensity. It is reported that there exists a threshold intensity below which no observable events of nucleation take place[40]. The nucleation probability increases linearly with the intensity and reaches to unity beyond a certain intensity[44]. The threshold intensity varies with the solute-solvent system.

- **Pulse frequency & duration**
  The laser-induced nucleation probability increases with an increase in pulse frequency up to a certain frequency. However, at a higher frequency, there are chances of solution heat-up which can reduce the supersaturation[45]. Furthermore, the nucleation probability can be increased by irradiating the sample with short pulse duration due to high peak intensity[44, 46].

- **Exposed volume**
  As the laser exposure volume increases the probability of impurities coming in the incident beam path of laser increases thereby resulting in higher nucleation probability (see 2.5.1.3). The exposed volume can be manipulated by varying the beam diameter of the laser pulse[45].

- **Wavelength**
  There is no definitive dependence of wavelength on nucleation probability or crystal properties[13]. However, the NPLIN experiments conducted by Ward et al.[40] for nucleation of KCl and KBr observed that the threshold intensity was lower at 532nm than at 1064nm of wavelength[40]. This was attributed to slight absorption of laser energy by solvent at 1064nm leading to decrease in local supersaturation. Therefore, a higher threshold intensity was required for NPLIN at 1064nm wavelength.

- **Aging**
  Aging refers to keeping the supersaturated samples at desired constant temperature for a definitive time before laser irradiation[40]. In early studies, it was suggested that aging of the sample was required (approximately 4-8 days) for the generation of large pre-clusters facilitating the NPLIN. However, later it was proved that the aging is not required for NPLIN[5]. Although, it has been reported that the nucleation probability increases with the aging of certain samples[30].

3

Solubility studies

"Our virtues and our failures are inseparable, like force and matter. When they separate, man is no more."

– Nikola Tesla

3.1. Motivation

The successful scale-up of any industrial process requires a good understanding of its parameter at the laboratory scale. Solubility is one of the crucial parameters required for better control over the crystallization process[47]. The solubility of a substance in any solvent depends on the temperature. It is very important to correlate solubility as a function of temperature to get good control over the crystallization process. This correlation also provides information on the temperature sensitivity of chemical compounds, which is crucial in determining the type of crystallization technique to use. This information can also be used to make a solution with various supersaturation to study the crystallization process.

3.2. Materials & Methods

The nitrogen was used to dry beakers, vials, and spatulas. The known quantity of potassium chloride (Sigma Aldrich, molecular biology, 99.0%) was dissolved in ultrapure water (ELGA Purelab, UK, 18.2 MΩcm) in small vials of 1.5mL. In this way, four known concentrations of aqueous KCl solution were prepared in sixteen vials with four vials holding the same concentration. A magnetic stirrer was placed inside each vial for mixing. The solubility experiments were performed using Crystal16 (Avantium) equipment, which is equipped with 16 (4x4) parallel reactors each of standard 1.5ml vials in four aluminium blocks. The temperature is controlled via electrical heating and cooling by peltier elements and a cryostat. The working principle of Crystal16 is based on the turbidity measurement of the solution inside vials. It has a laser that transmits light across the solution in vials and indicates the onset of nucleation and dissolution by the change in transmission.

3.2.1. Solubility Test

The solubility of potassium chloride in water was determined by finding the clear point temperature at different concentrations of salt. The clear point is defined as the temperature at which a clear solution is obtained for a particular concentration. The experiment was performed by preparing four different known concentrations of the solution in sixteen vials with four vials holding the same concentration. All vials were placed in Crystal16. Each vial was stirred using a magnetic stirrer at 700 rpm. The solution was heated at the rate of 0.05°C/min till it reaches 40°C, held for 5 minutes, and then ramped down at the rate of 0.3°C/min till it reaches 10°C. This user-defined heating and cooling cycle is repeated three times. As shown in Figure 3.1, the blue line represents the temperature cycle and the red line represents the transmission. The temperature at which the transmission rises from 0% to 100% is attributed to the clear point temperature of the solution at which the solute completely undergoes dissolution.

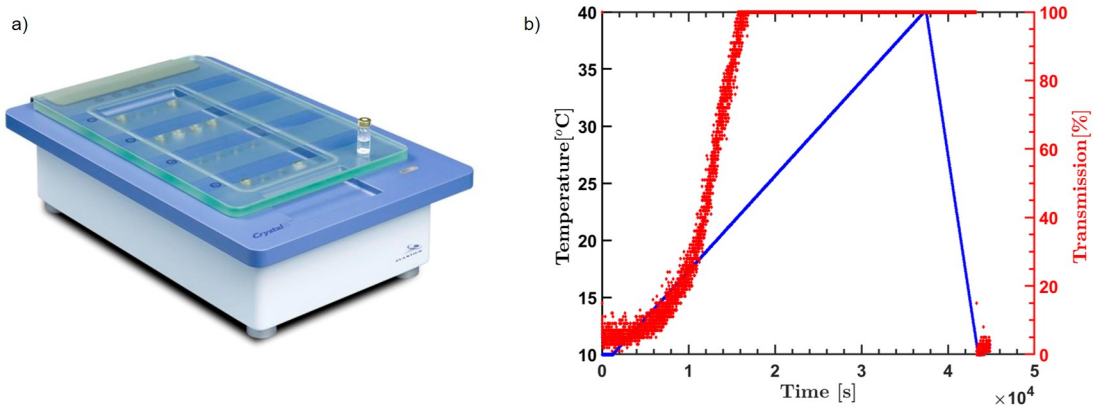

Figure 3.1: a)Crystal16, Avantium is a multiple 16 reactor station used for performing solubility experiment, b) The temperature profile with transmission recorded by crystal16.

3.3. RESULTS AND DISCUSSION

The solubility of aqueous potassium chloride obtained from crystal16 for different concentrations is shown in Figure 3.2. It is reported in the unit of g solute/ 100g solvent and is fitted with a linear curve over the range of temperature. A slight variation in the solubility data recorded from our experiments was observed when compared to literature values[48]. The main reason for this difference can be attributed to the experimental protocol, the sensitivity of the equipment, purity of the chemical stock, solvent, and the nucleation kinetics, which here is reflected on the solubility curve. It is also worth noting that the heating rate used in our experiment is very low (0.05°C/min) to give crystals enough time to dissolve. This was done to improve the accuracy of clear points.

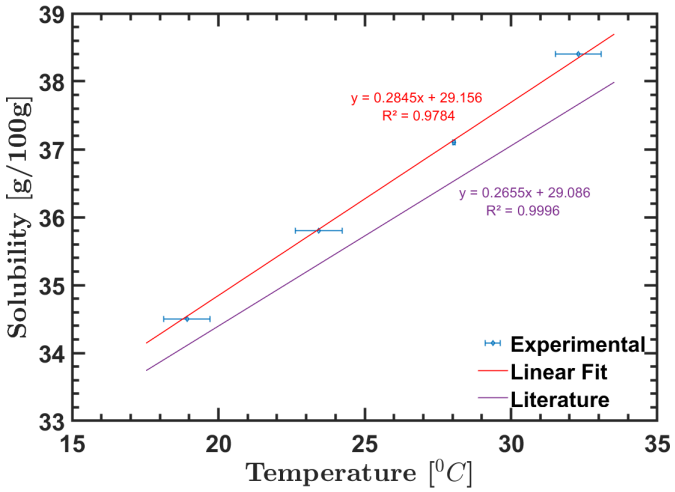

Figure 3.2: Solubility curve obtained experimentally is compared with literature[48].

Note that the KCl is highly soluble in water and its solubility increases with the temperature as shown in Figure 3.2. Depending on the process whether it is endothermic or exothermic, the temperature will have an effect on the solubility.

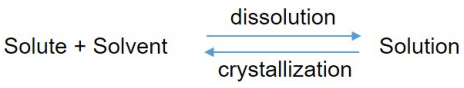

Figure 3.3: Dissolution equilibrium.

This is in accordance to Le-chatlier principle[49]. For endothermic process, the equilibrium as shown in Figure 3.3 will shift towards the right side with increase in temperature and thus, increasing the solubility. In literature, it is found that the dissolution of KCl in water is endothermic process. Hence, the solubility of KCl in water increases with the temperature.

3.4. CONCLUSION

The solubility curve of aqueous KCl was obtained by using Crystal16. It is one of the fundamental properties providing valuable information about the supersaturation of KCl at different temperatures. The future experiments will be carried out by the same chemical stock, thus the solubility curve obtained from our experiments will be used throughout this research.

4

Cooling crystallization

"Every brilliant experiment, like every great work of art, starts with an act of imagination."
– Jonah Lehrer

4.1. Motivation

Batch cooling crystallization can be used to study nucleation kinetics which will serve as a control experiment to the NPLIN experiments that follow. Therefore, the induction time of various supersaturated solutions of potassium chloride will be studied. The induction time is defined as the time duration between the constant supersaturation achieved and the moment when first crystals appear[50]. There will be variation in the induction time due to the stochastic nature of nucleation and this can be used to estimate the nucleation kinetics in solutions under realistic industrial experimental conditions[51].

This chapter will mainly familiarize the reader with the setup developed to conduct the batch cooling crystallization along with the explanation of the results.

4.2. Materials and Methods

4.2.1. Sample Preparation

The supersaturated solution was prepared by analytically weighing the potassium chloride (Sigma Aldrich, molecular biology, 99.0%) in Ultrapure water (ELGA Purelab, UK, 18.2 MΩ cm) using the solubility data obtained in section 3.3. The solution was prepared directly inside the batch reactor to minimize errors that can occur while transferring the solution from one container to another. The prepared solution was mixed using a stirrer and heated inside the batch reactor at 35°C for two hours to obtain a clear solution. The bulk solution was undersaturated at 35°C. The details of batch reactor components are explained in the subsequent subsection 4.2.2. All samples of different supersaturation (SS = 1.0027, 1.0074, and 1.0122 measured at 26°C each) were prepared in the same manner.

4.2.2. Setup

The experiments were conducted in a glass jacketed batch crystallizer (1L capacity). The mixing was done mechanically by a 45° pitch blade turbine impeller driven by an electrical motor (Heidolph RZR 2102 control) as shown in Figure 4.1. The bulk temperature was monitored by a thermocouple (Pt-100), controlled by a thermostatic bath (Lauda, ECO Gold RE 1050) using water circulation inside the crystallizer jacket. An additional thermocouple (Type K) was used to record bulk temperature using an eight-channel thermocouple data logger (Pico Technology USB TC- 08). The online process monitoring was done by Process Analytical Tools (PAT) like Focused Beam Reflectance Measurement (FBRM)(Mettler Toledo, BV), and an online camera (Smart Online Particle Analysis Technology - SOPAT GmbH).

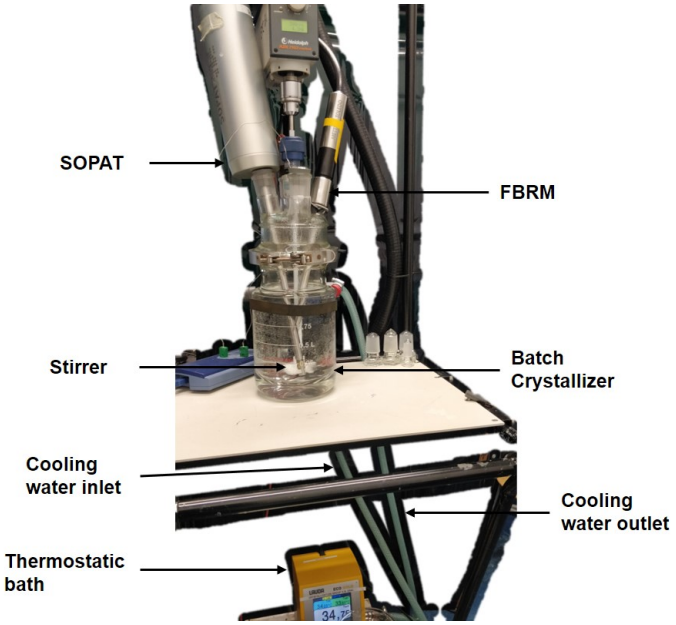

Figure 4.1: The setup for batch cooling crystallization in liter volume scale placed over moveable frame.

4.2.2.1. FBRM

The FBRM probe, model G400 (Mettler Toledo) provides the online measurement of particle count and chord length distribution of the particle. A focused laser beam moving in a circular path with a tangential velocity of 2 m/s is emitted through the sapphire window as shown in Figure 4.2. When a particle is detected in the direction of the laser at the tip of probe, the laser is reflected back into the probe. The probe treats each instance of this occurring as a single particle detection. The product of pulse width (time) and tangential velocity gives the chord length[52].

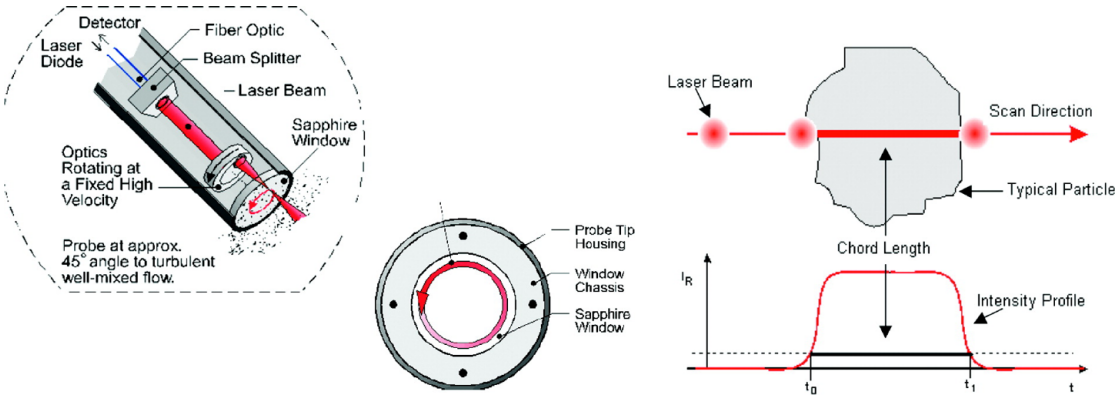

Figure 4.2: The schematic of the internal optics and working principle of FBRM. Image taken from literature[53].

The iC FBRM software (version 4.4) captures the data with an option to select from primary and macro mode. These modes allows the user to change the instrument's sensitivity according to the aspects of the dispersed phase. In primary mode, it is very sensitive to even small fines or bubbles present in bulk whereas, in macro mode, it provides a digital filter that reduces the noise generated in the reflection signals as shown in Figure 4.3[54]. In the current system, the macro mode was selected (sampling interval of 5 seconds) to reduce signal fluctuations due to slight variations in the bulk system generated by tiny bubbles. The angular position of the probe plays a significant role in particle detection. The probe was placed at an angle of 45° to liquid surface such that the sapphire window sees maximum particles[52]. Here, FBRM is used to detect the onset of nucleation events, and chord length distribution is not used for particle size distribution.

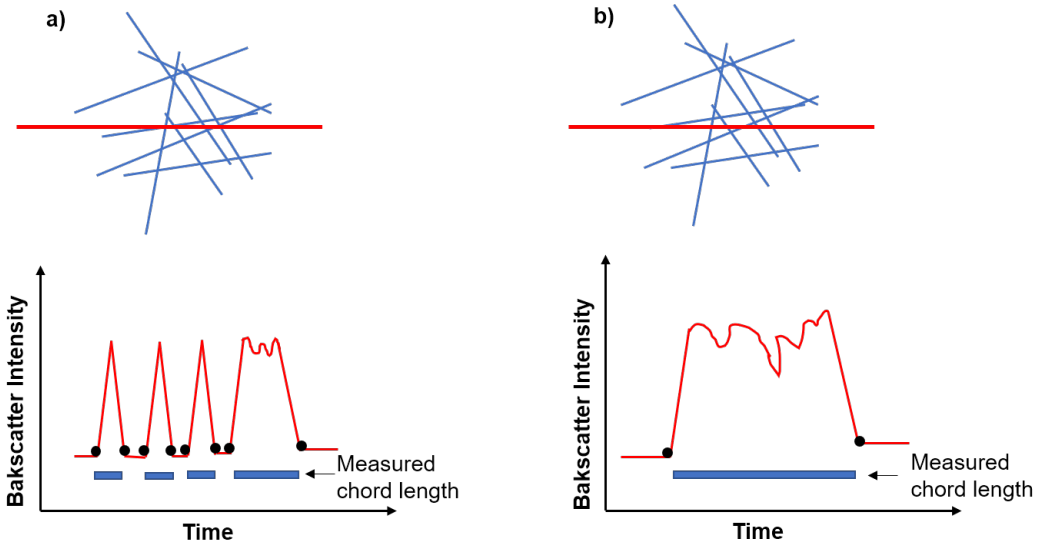

Figure 4.3: The schematic representing a) primary mode, b) macro mode of FBRM. Image adapted from literature[54].

4.2.2.2. SOPAT

The SOPAT imaging device consists of a probe with a tip diameter of 12 mm and a central workstation with a graphic user interface (GUI) that allows image acquisition and analysis. The probe has integrated fiber optics that provide illumination for the particles to be imaged by manipulating strobe intensity. The advanced optics inside it allows for the specifications mentioned in Table 4.1. In addition, the focal plane can be fine-tuned for sharp images, and the frame rate can be adjusted from 0.1 to 20 Hz[55]. In this research, a frame rate of 5 Hz was sufficient to capture images, and the focus point was set between 120-250 μm. The acquired images can be processed using a built-in image processing algorithm via GUI.

Table 4.1: Specification of SOPAT

Specification	Value
Measuring range	3-350mm
Field of view	800mm
Depth of view	200mm
Resolution	228cpmm
Frame rate	0.1-20Hz

Figure 4.4: The SOPAT imaging system. Image courtesy: SOPAT GmbH.

4.2.3. EXPERIMENTAL PROCEDURE

The solution was subjected to a temperature profile as shown in Figure 4.5. It was maintained at 35°C for two hours to completely dissolve solute in the solution. In preliminary experiments, the solution temperature was elevated up to 50°C, which led to a significant amount of solvent evaporation (≈10 g), thus changing the supersaturation significantly. Therefore, the maximum temperature was adjusted to 35°C, and solvent loss due to evaporation at this temperature was negligible (≈1 g) compared to the loss at 50°C. After that, the solution was cooled at a linear cooling rate of 0.3°C/min to the target temperature of 26°C. The target temperature was chosen in such a way that crystallization does not occur during the cooling phase[51]. The temperature profile and cooling rate, as stated in section 2.4, play an important role in the nucleation and growth rate of crystals. Hence, the temperature profile was followed strictly using the thermostatic bath.

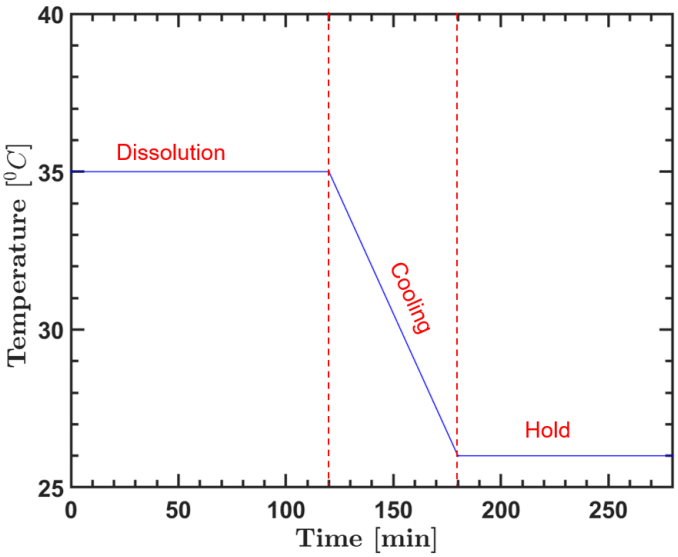

Figure 4.5: Temperature profile with linear cooling rate of 0.3°C/min.

The stirring rate was maintained constant at 300 rpm throughout the experiment. Since the stirring rate can influence the nucleation (see section 2.4), an optimal stirring rate was chosen from the literature[4] to maintain a homogeneous condition in the bulk while limiting the effect of secondary nucleation due to mechanical agitation.

A constant supersaturation was maintained at the target temperature of 26°C (referred to as time zero) until the onset of nucleation. The onset of nucleation was recorded by FBRM through a sudden increase in the number of counts of the particles detected as in Figure 4.6. The time difference between the moment when FBRM detects crystal and time zero was taken as induction time. The morphology of the crystals generated was captured by the online camera probe SOPAT. Experiments were repeated 10 times to improve statistics.

4.3. RESULTS AND DISCUSSION

4.3.1. INDUCTION TIME

Figure 4.7 shows the average induction times for three supersaturation values of KCl: SS = 1.0027, 1.0074, 1.0122. Shorter induction times were recorded with higher supersaturations and vice-versa. The vertical error bars represent the standard deviation in induction time obtained from 10 repetitions.

Although there was a good control over the temperature, concentration, and volume of the bulk solution, there was variation in induction time for each supersaturation. Note that the uncertainty of induction time was higher at lower supersaturation. This uncertainty can be attributed to the stochastic nauture of the nucleation and it contains important information about nucleation kinetics[56]. These variations in induction time at constant supersaturation are reported for other compounds also in the literature[57].

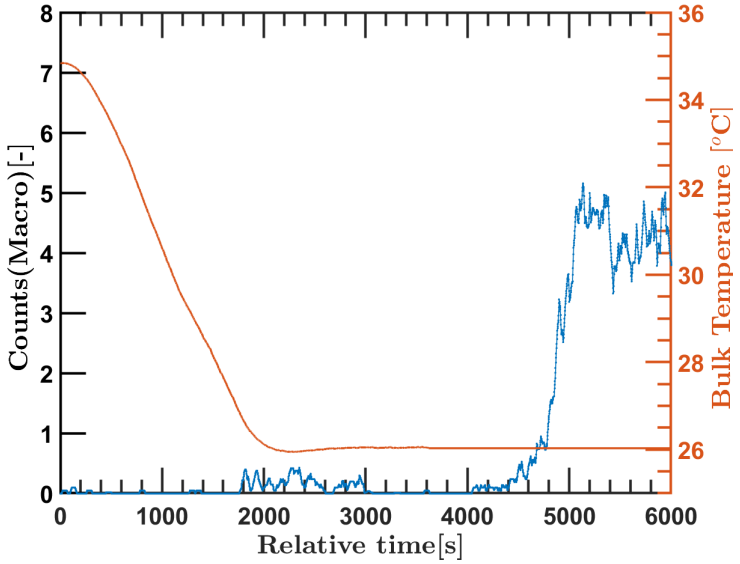

Figure 4.6: The onset of nucleation recorded by FBRM for control experiment of KCl solution.

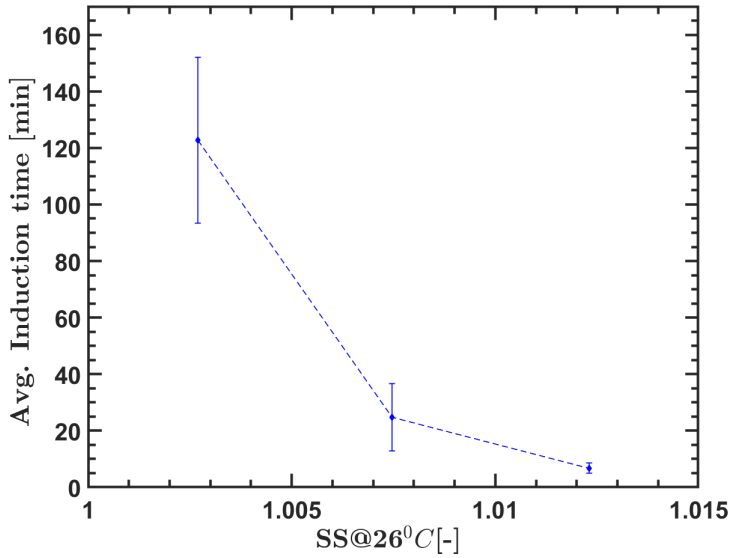

Figure 4.7: Average induction time for SS = 1.0027, 1.0074 and 1.0122

Note that the induction time decreases very steeply as the supersaturation increases. This can be explained by the fact that supersaturation is the driving force for nucleation and as the supersaturation increases the probability of nucleation also increases corroborating with the literature[56].

5

NPLIN Experiment

"The good thing about science is that it's true whether or not you believe in it."

– Neil deGrasse Tyson

5.1. Motivation

This chapter includes the non-photochemical laser-induced nucleation experiments. In preliminary experiments, an LED source was used to conduct the NPLIN experiments but it gave an inconclusive result (see Appendix A). Thus, Nd:YAG laser was used as a light source to conduct the NPLIN experiments. This chapter entails different experiments conducted apart from conventional NPLIN experiments as explained in subsequent subsections. It is reported in the literature[44] that NPLIN takes place above a particular intensity known as threshold intensity which mainly depends on the supersaturation and the volume of exposure. Therefore, the threshold intensity at each supersaturation value (SS = 1.0027, 1.0074, and 1.0122) is experimentally evaluated in this project. The induction time measurement is done for each supersaturation. NPLIN experiments are also conducted in undersaturated solutions. The effect of the number of laser pulses is investigated. Finally, the particle size distribution of crystals formed by NPLIN experiments is compared to the control experiment.

5.2. Materials and Methods

The sample preparation protocol was same as mentioned in subsection 4.2.1 and the bulk solution was prepared for three supersaturation values: SS= 1.0027, 1.0074, and 1.0122. The same setup as shown in Figure 4.1 was used to perform NPLIN experiment after incorporating laser as shown in Figure 5.1. Nd:YAG (Continuum Powerlite DLS 8000 model) nanosecond pulsed laser with following properties in Table 5.1 was used for the NPLIN experiments.

Table 5.1: Q-Switched Nd:YAG laser properties

Properties	
Wavelength	532nm
Frequency	10Hz
Single pulse duration	7ns
Width of beam	9mm

In this experimental protocol, batch cooling crystallization was combined with a conventional NPLIN experiment. The solution was subjected to the same temperature profile as shown in Figure 4.5, and the laser was irradiated horizontally in the bulk solution at the target temperature of 26°C. The laser beam was adjusted in such a way that it would not hit the stirrer in order to avoid any impurity falling in bulk solution from the stirrer due to laser ablation.

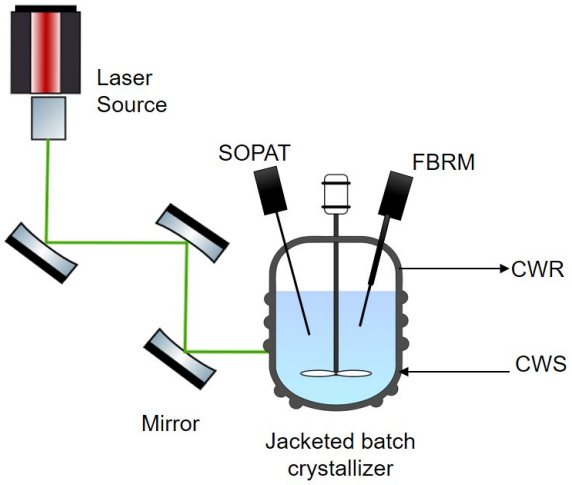

Figure 5.1: The schematic for NPLIN experiments on batch crystallizer in liter volume scale.

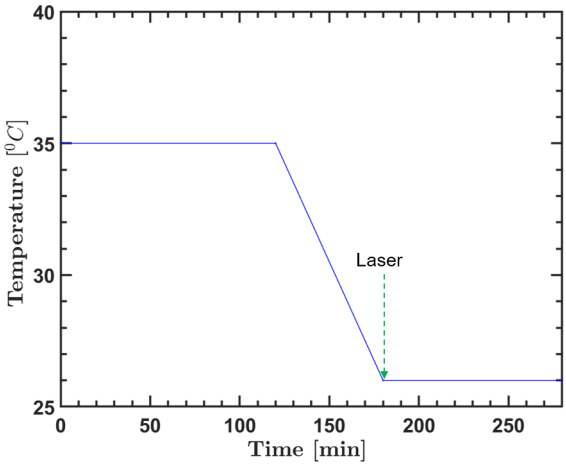

Figure 5.2: The temperature profile for NPLIN experiments on batch crystallizer.

5.2.1. PARTICLE SIZE DISTRIBUTION

An offline technique was used to do a comparative study of the particle size distribution for control and NPLIN experiments. The sample preparation for PSD analysis was done as follows:

- The sample was collected after a residence time of 5 min. The residence time, here, refers to the time duration between the onset of nucleation and sample collection. The sample (around 900mL) was taken out by siphoning the suspended crystals such that maximum crystals were encountered.
- The collected sample was filtered using vacuum to obtain crystals.
- The crystals obtained in previous step were washed with isopropanol solvent.
- The prepared sample was analyzed for PSD using Microtrac S3500 (Montgomeryville, PA, USA) in wet mode using isopropanol as the carrier fluid.

5.2.1.1. MICROTRAC S3500

This instrument works on the principle of laser diffraction mechanism consisting of three laser sources and two detectors as shown in Figure 5.3 (b). This allows detecting the scattered light from the forward low angle region to almost the entire angular spectrum (up to 163°). In each measuring cycle, laser 1 gets activated and passes through well-dispersed sample particle while laser 2 and 3 remain inactivated, and the scattered light is detected by on-axis and off-axis detectors. Similarly, laser 2 and 3 gets activated one at a time and scattered light is detected by on-axis and off-axis detectors. Thus, the tri-laser system provides the measure-

ment of scattered light by different optical pathways. Particle size distribution is generated by combining the final scattered light information from all laser sources.

The data is continuously collected by the Microtrac FLEX software and analyzed by using modified Mie's scattering theory, generating PSD for both spherical and non-spherical particles. Moreover, this GUI software allows the user to check volume, area, and number-based distributions along with percentile and other statistical data.

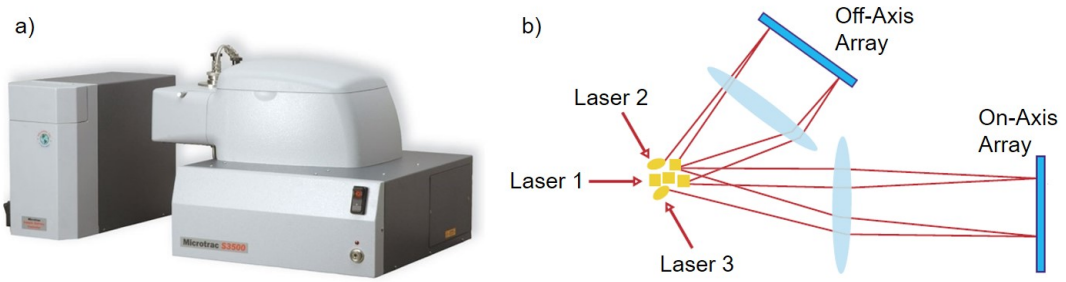

Figure 5.3: a)Microtrac S3500, b) The schematic representing the tri-laser system. Image courtesy: Micotrac MRB

This technology has an analysis time of 10 to 30 seconds and works in the size range of 0.02 to 2800 μm. It allows the user to choose between dry and wet modes depending on the sample. The wet mode is used in this study, with isopropanol as the carrier fluid. In addition, it also has a built-in sonicator, which was used to sonicate the sample for one minute before analysis to ensure that all particles were suspended separately.

5.3. Results and Discussions

5.3.1. Threshold Intensity

The threshold intensity of NPLIN as a function of supersaturation was determined by irradiating the solutions with 300 pulses at the wavelength of 532 nm as shown in Table 5.2. The error in threshold intensity is due to the fluctuations of the laser power measured by the powermeter (Gentec-EO Maestro). The threshold intensity varies with supersaturation following the previous reports in literature[5, 13]. It can be observed that lower supersaturation has higher threshold intensity for NPLIN. According to classical nucleation theory, the nucleation rate is non-linearly dependent on the supersaturation and the nucleation probability is significantly lower at low supersaturation. Hence, a strong electric field is required for NPLIN. This is evidence corroborating the isotropic electronic polarization mechanism hypothesis[13] (see 2.5.1.2). However, this threshold intensity is not solely dependent on supersaturation but also on laser pulses. Thus, the reported threshold intensity may vary as a function of the number of pulses for each supersaturation.

Table 5.2: NPLIN threshold intensity for various supersaturation value at 26°C with 300 laser pulses and at wavelength of 532nm

SS at 26°C	Threshold intensity (MW/cm^2)
1.0027	44.99±2.25
1.0074	4.05±0.11
1.0122	2.92±0.04

5.3.2. Induction Time

The induction time for the NPLIN experiment is recorded using FBRM and SOPAT for three supersaturation values. Figure 5.4 (a), shows the FBRM data for NPLIN and control experiment for an experiment of SS = 1.0027. Figure 5.4 (b) represents the induction time comparison of NPLIN at SS = 1.0027, 1.0074, and 1.0122. Note that, it is a semi-log plot to highlight the order of magnitude difference in induction time of NPLIN and control experiments. The same properties of the laser beam are used for all supersaturation

mentioned in Table 5.3. It can be observed that the induction time is an average of 2 min for NPLIN experi-

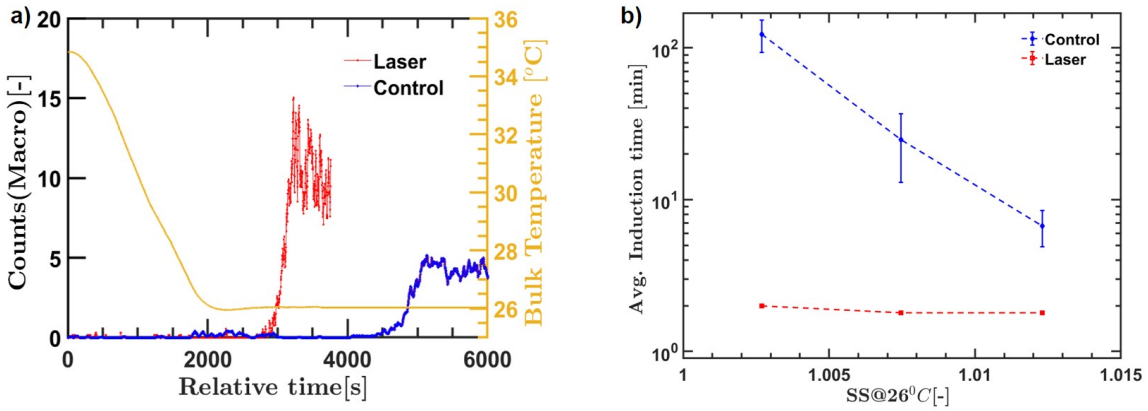

Figure 5.4: a) The number of crystals recorded by FBRM for NPLIN and control experiment. b) The induction time for various supersaturation of NPLIN and control experiments.

Table 5.3: The properties of laser used for NPLIN experiments for SS = 1.0027, 1.0074, and 1.0122 at 26°C.

Properties	
Intensity	45MW/cm^2
Number of Pulses	300
Wavelength	532nm
Frequency	10Hz
Single pulse duration	7ns
Width of beam	9mm

ments indicating that the crystals are formed immediately after irradiating the supersaturated solution, and there is a notable decrease in the induction time of NPLIN as compared to control experiments mentioned in chapter 4. This difference is maximum at the lowest supersaturation value of 1.0027. It is mentioned in the literature that the potassium chloride solution is transparent for 532 nm wavelength[13]. So the supersaturation variation due to the absorption of light is ruled out. The reduction in induction time can be explained by isoelectronic polarization and nano-particle heating mechanism (see 2.5.1.2, 2.5.1.3) as mentioned in literature[5]. Moreover, it can also be noted that the induction time of NPLIN is at an average of 2 min irrespective of the supersaturation value and it does not depend on laser intensities. This can be due to the intensity used for NPLIN (45 MW/cm^2) is higher than the threshold intensity for SS = 1.0074 (4.05 MW/cm^2) and 1.0122 (2.92 MW/cm^2) that is enough to induce nucleation[5].

5.3.3. SINGLE PULSE VS MULTIPLE PULSE

The effect of the number of pulses on NPLIN is investigated experimentally by irradiating single and multiple pulses independently. These experiments were performed using a supersaturation of 1.0027 because the induction time of control experiment is maximum at SS = 1.0027 as compared to other supersaturation, thus the solution is quite stable. The following laser property in Table 5.3 except the number of pulses was used for the control and NPLIN experiment. With the single pulse, very fewer crystals (3-4) were detected by FBRM at 4500s as shown in Figure 5.5. The delay in detection time of crystals by FBRM can be attributed to the less number density of crystals formed in 1L volume. Whereas, with multiple pulses, a comparatively higher number of crystals were formed immediately as shown in Figure 5.5.

Contrarily, Irimia et al.[45] performed the NPLIN experiment on supersaturated aqueous glycine solution and did not observe any significant change in nucleation probability with multiple pulses as compared to the single pulse. The reason can be attributed that they have allegedly exposed the same volume to multiple pulses in a vial. In contrast, in a batch crystallizer, the exposed volume varies due to stirring, resulting in a higher exposed volume by the laser beam with 300 pulses than with a single pulse.

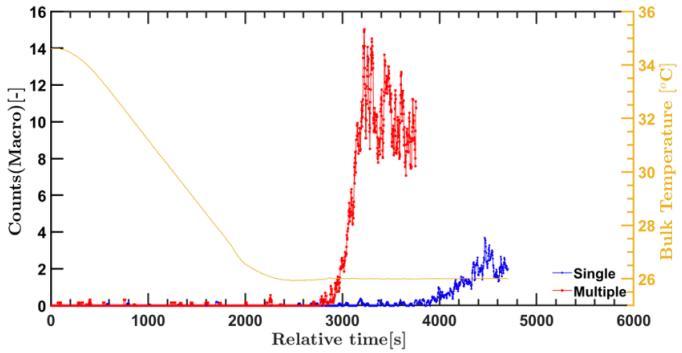

Figure 5.5: The number of crystals recorded by FBRM for single and multiple (300) pulses

5.3.4. NPLIN IN UNDERSATURATED SOLUTION

This experiment is inspired by the double pulse method available in literature[58]. Galkin et al.[58] used this method to separate the nucleation from ensuing growth. In this study, the temperature of a supersaturated protein solution was increased after a fixed period of time, resulting in a decrease in supersaturation of the solution that was low enough to prevent further nucleation while enabling existing crystals to expand to detectable size.

As shown in Figure 5.6, the solution was dissolved at 35°C and subjected to a linear cooling rate of 0.3°C/min. The laser was irradiated at undersaturated condition (SS = 0.98 at 27°C) and then supersaturation was increased (SS = 1.001) by lowering the temperature to 26.5°C. This was done to make sure that the nuclei supposedly formed in undersaturated conditions can grow. The property of the laser was the same as given in Table 5.3.

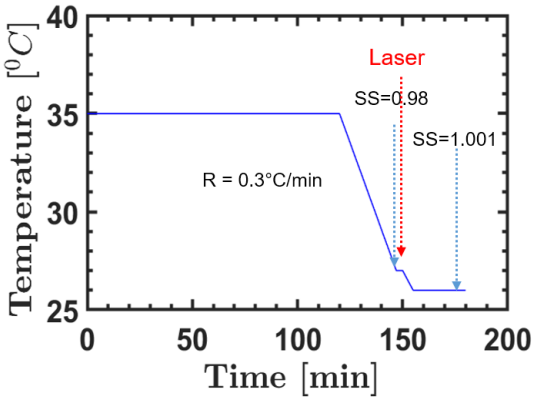

Figure 5.6: The temperature profile for performing NPLIN experiment in undersaturation condition

A control experiment was conducted in which the solution was subjected to the cooling profile as shown in Figure 5.6. The FBRM data as shown in Figure 5.7 confirms that there were no crystals nucleated till 3400s (≈ 25 min after achieving SS = 1.001), indicating that the solution was quite stable and there was no spontaneous nucleation.

In NPLIN experiment, the solution was subjected to the same cooling profile as shown in Figure 5.6 and the laser was irradiated at undersaturated condition (SS = 0.98 at 27°C). FBRM detected the crystals supposedly formed in undersaturated condition and later grown in supersaturated condition when temperature was reduced to 26.5°C. This experiment was conducted for three repetitions. It is noteworthy to point out that the solution at 27°C can be saturated due to uncertainty in solubility curve. However, the control experiment confirms that the solution was stable and there was an effect due to NPLIN. At this stage, it is

speculated that the non-observable clusters formed due to laser irradiation in undersaturated condition grow into detectable crystals in the supersaturated solution.

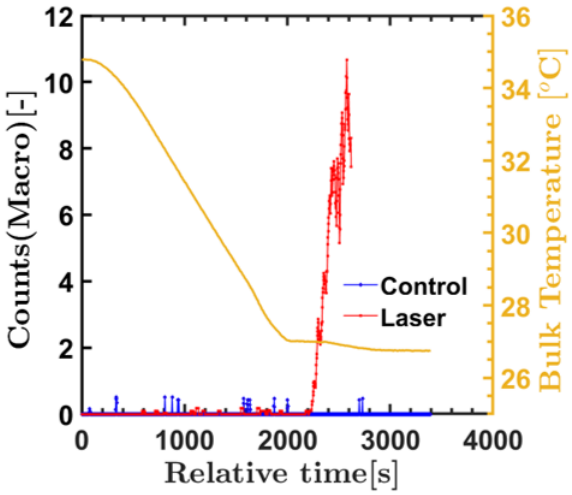

Figure 5.7: The FBRM data for NPLIN experiment and control experiment.

5.3.5. PARTICLE SIZE DISTRIBUTION

It is mention in the literature that the sample preparation technique for PSD analysis affects the observed PSD[59]. However, the same sample preparation protocol and offline technique were followed for the PSD obtained for control and NPLIN experiments as mentioned in subsection 5.2.1. The PSD obtained using laser diffraction is expressed using volume based distribution. All PSD in this report are expressed as the percentage volume fraction (q_{43}%) in each channel of Microtrac, and the mean diameters are calculated as volume weighted mean diameter (d_{43}) given by the Equation 5.1.

$$d_{43} = \sum_{c=1}^{N} n_c d_c^4 / \sum_{c=1}^{N} n_c d_c^3, \tag{5.1}$$

where d_c is the diameter of the particle in the c^{th} sampling interval of instrument and n_c is the number fraction of the particle. The laser properties are same throughout the NPLIN experiments: wavelength of 532 nm and 300 pulses.

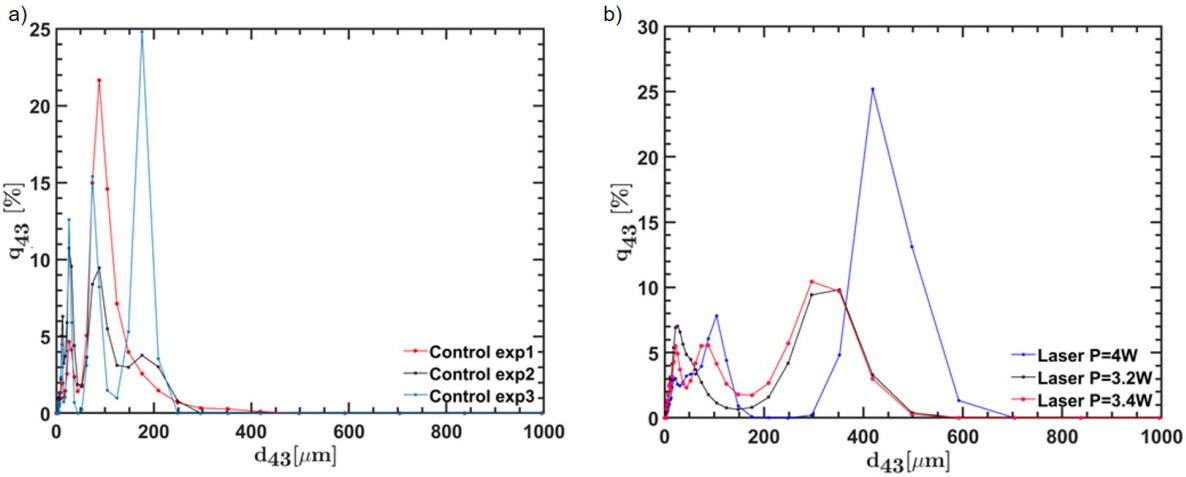

Figure 5.8: a) PSD for various independent control experiments, b) PSD for various NPLIN experiments. Both graph corresponds for supersaturation value of 1.0027 at 26°C.

Figure 5.8 (a) represents the PSD obtained from control experiments i.e., batch cooling crystallization. It can be observed that the nature of PSD obtained from all repetitions of control experiments are different each time as expected owing to the stochasticity of spontaneous nucleation, and the dominant size of crystals is in the range of 100-200 μm. It is reported in the literature that the cooling rate affects the PSD and linear cooling rate results in PSD with a low mean average size of particles[4, 24].
Figure 5.8 (b) represents the PSD obtained from NPLIN experiments. It can be observed that the nature of PSD obtained is the same with the dominant size in the range of 300-500 μm.

This indicates that the nucleation rate is dominant in control experiments whereas, the growth rate is dominant in NPLIN experiments. It is also worth noting the weight of the dried crystals that was taken after 5 mins of the first crystal observed. This indicates the degree of supersaturation consumed in both types of experiments. It can be observed from Table 5.4 that the weight of excess KCl solute at 26°C is 1.01g and out of which only 0.435g of crystals were formed in control experiments, indicating less supersaturation consumption, whereas, in NPLIN experiments, 0.503g of crystals were formed indicating higher supersaturation consumption.

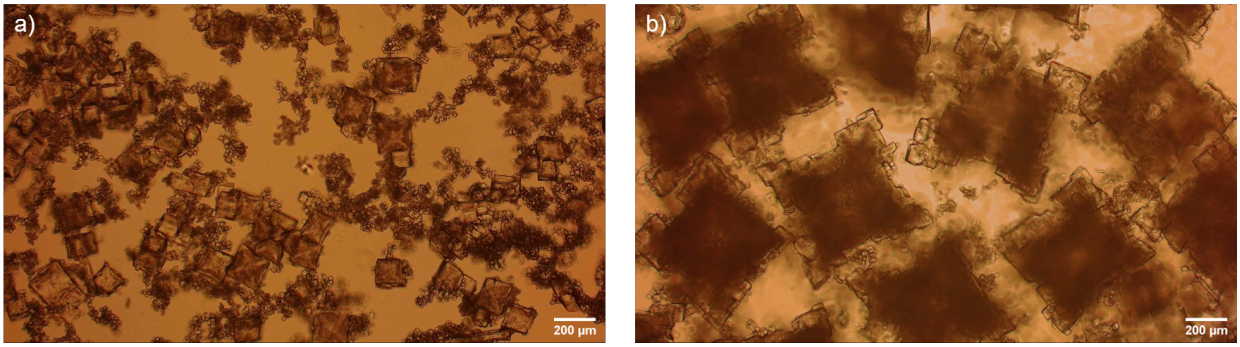

Figure 5.9: Microscopy image of KCl crystals from a) Control experiment, b) NPLIN experiment.

Figure 5.9 (a) and (b) represents the optical microscopy images of crystals formed in the control and NPLIN experiment respectively taken under ZIESS inverted microscope (10X 0.25DIC objective lens). In Figure 5.9 (a), it can be observed that there is a dominant size of crystals along with smaller fines that can be generated due to attrition, and breakage of crystals owing to impact from stirrer. This explains the reason for multimodal PSD. Moreover, the higher dominant size of crystals in the optical microscopy image of NPLIN can be observed corroborating with the previous PSD result obtained from Microtrac. It is also worth noting that the optical microscopy image of the NPLIN experiment shows hopper growth around the edges. In the literature, such hopper growth is observed in cubic crystals with high growth rate[60]. In other words, the effective supersaturation consumption is more corroborating with the weight of the dried crystals shown in Table 5.4.

Table 5.4: Weight of dry sample taken from the crystallizer after a residence time of 5 min.

Weight of excess KCl at 26°C (g)	Weight of dry KCl crystals (g)	
	Control Experiment	NPLIN Experiment
1.01	0.435	0.503

Figure 5.10 (a) and (b) represents the PSD comparison at SS = 1.0027 and 1.0074 obtained in control and NPLIN experiments respectively. The PSD for higher supersaturation also exhibits a similar trend. It should be noted that the dominant size in the control experiment for SS = 1.0074 is higher which can be explained by the fact that the growth of the crystals is linearly dependent on the supersaturation[4]. Note that the dominant peak of SS = 1.0027 and 1.0074 lies on the same size which can be an indication that the laser can be used to control the PSD.

From Figure 5.8, and Figure 5.10, a clear shift in peaks of dominant size is observed. This shift in peaks is reported in seeded crystallization where the growth of the seeds takes place in metastable region[61, 62]. Narducci et al.[63] investigated the use of short ultrasonic burst on batch cooling crystallization of aqueous

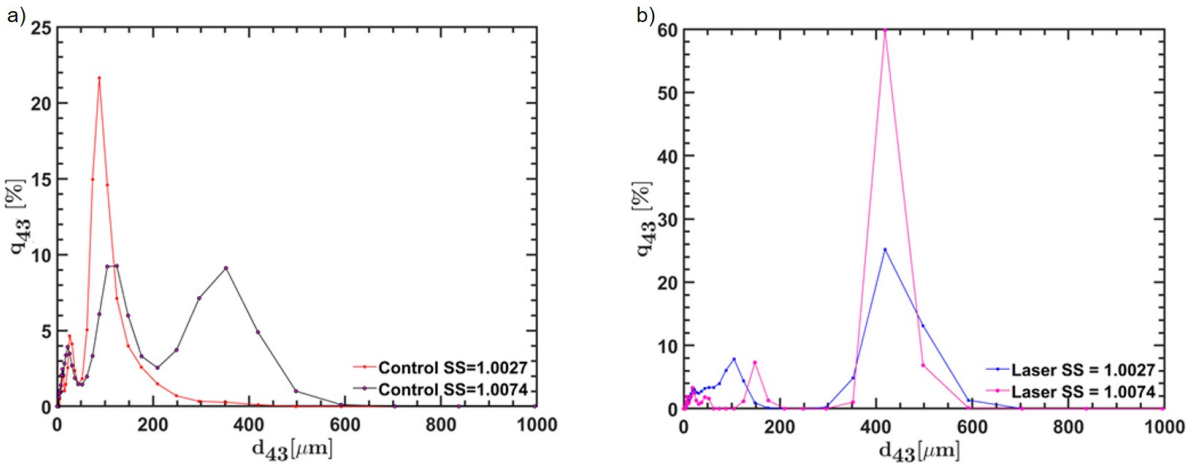

Figure 5.10: a) PSD for control experiments for SS = 1.0027, and 1.0074 at 26°C, b) PSD for NPLIN experiments for SS = 1.0027, and 1.0074 at 26°C and laser power of 4W.

adipic acid and reported the growth dominant PSD comparable with the PSD of conventional seeding crystallization. At this stage, it can be hypothesized that the laser is generating seeds that grow in the metastable region resulting in growth dominant PSD. However, this hypothesis needs further validation by modelling. This can be done by population balance modelling and comparing the nucleation kinetics obtained from modelling of control and NPLIN experiments[64].

6

Conclusion and Recommendations

"I am enough of the artist to draw freely upon my imagination. Imagination is more important than knowledge. Knowledge is limited. Imagination encircles the world"

– Albert Einstein

6.1. Conclusions

This research aims to provide proof of concept for batch cooling crystallization with NPLIN. A setup was developed to conduct control experiments and compared them with NPLIN. After conducting control experiments it was found that there exists a minimum crystal number density for online process tools (FBRM, SOPAT) to detect particles effectively. The induction time measurement was done experimentally and it reduced drastically with the increase in supersaturation, indicating the higher nucleation probability.

Initially, LED was used as the light source for NPLIN experiments but it gave an inconclusive result (see Appendix A). Later, it was replaced with Nd:YAG nanosecond pulsed laser to perform NPLIN experiments. Firstly, it confirmed that there exists a minimum threshold intensity for NPLIN to take place at given conditions of laser properties and solution volume. Furthermore, it was observed that there was a drastic reduction in induction time of NPLIN experiments than the control experiments. NPLIN found effective especially in low supersaturation to reduce the induction time. This gave an optimistic view about more spatiotemporal control over nucleation using NPLIN. Moreover, the number of laser pulses played a significant role in the number of crystals generated. The number of crystals generated at 300 pulses was found to be higher than that of a single pulse. Hence, laser properties like power, number of pulses can be used to tame the nucleation. NPLIN experiments in undersaturated solution indicated that the crystals supposedly nucleated can grow into observable crystals provided there was solute available for growth.

Finally, PSD analysis was done by an offline technique. There was a shift in peaks of the dominant size of crystals in the PSD of NPLIN as compared to control experiments. The degree of supersaturation consumption by NPLIN was more than the control experiment, confirmed from the weight of the dried crystals after crystallization process. This lead to the hypothesis that the laser was generating seeds that are possibly growing into larger crystals. Additionally, the similar PSDs generated in NPLIN experiment repetitions give a positive outlook about controlling the PSD using the laser at particular power.

To summarize, NPLIN allows enhancing the nucleation kinetics in a more controlled manner. However, the NPLIN as a process requires further study by dual approach combining experiment and simulation to utilize its full potential.

6.2. Recommendations

A better understanding of NPLIN at pilot scale could be achieved by carrying out further experiments. These recommendations include,

* **Strengthening with more statistical data**
  The results of induction time for the batch cooling experiment are inferred from 10 experiments for each supersaturation. More repetitions of these experiments give more data points, that can be used to derive nucleation kinetics using classical nucleation theory.

* **Better image acquisition**
  There exists a threshold crystal number density for SOPAT to capture the image with sharp features. The existing probe fails to acquire sharp images at low supersaturations used in this work and augmentation of supersaturation is limited by the stability of the solution. Additionally, the size of KCl crystals is found bigger than the size range of SOPAT (3-350μm) that poses a problem to capture images with all edges. Moreover, the GUI software of SOPAT for post-processing does not allow the implementation of user-defined functions according to particle size and shape. It will be better if a suitable inline camera (for example, EasyView Mettler Toledo) be used to capture sharp images. These acquired images can be used to generate particle size distribution by image analysis. This will further help to understand the development of particle size distribution throughout the growth of crystals.

* **Use of laser fiber for performing NPLIN experiments**
  More experiments with a continuous source of light can help in understanding its effect on the induction time of nucleation. In comparison to LED light, fiber laser will be easier to focus its collimated beam to achieve the NPLIN threshold intensity reported in literature[13].

* **Effect of parameters on PSD**
  The PSD is obtained by offline technique and a residence time of 5 min is maintained after crystal formation. The effect of parameters like residence time for sample acquisition, the laser energy, and the number of pulses can be varied as parameters to see its effect on PSD.

* **Modelling for PSD**
  It is proposed that the laser is generating seeds that are growth dominant. This idea can be consolidated by the modelling of PSD generated by control and NPLIN experiments. One of the methods can be based on population balance to generate PSD and compare it with experimental results.

Appendices

A

LED Experiment

A.1. Motivation

This experiment aims to induce nucleation by using light source in the batch cooling crystallizer and compare the induction time with the control experiments. LED is used as the continuous light source. This chapter encompasses the experimental protocol, the challenges, and the discussions for the results obtained.

A.2. Material and Methods

The main components used in this experiment are given below:

- Potassium chloride (Sigma Aldrich, molecular biology, 99.0%)
- Ultrapure water (ELGA Purelab,UK, 18.2 MΩcm)
- Nitrogen to dry beakers, vials and spatulas
- UV fused Silica Plano-Convex lens, Uncoated (f = 60.2 mm, Ø2")
- High-Power LED for Microscopy (SOLIS-415C from Thorlabs, Inc.)

The sample preparation technique was the same as mentioned in subsection 4.2.1 and the LED experiments were conducted on the same setup as mentioned in subsection 4.2.2. A schematic representation of the experimental procedure is depicted in Figure A.1

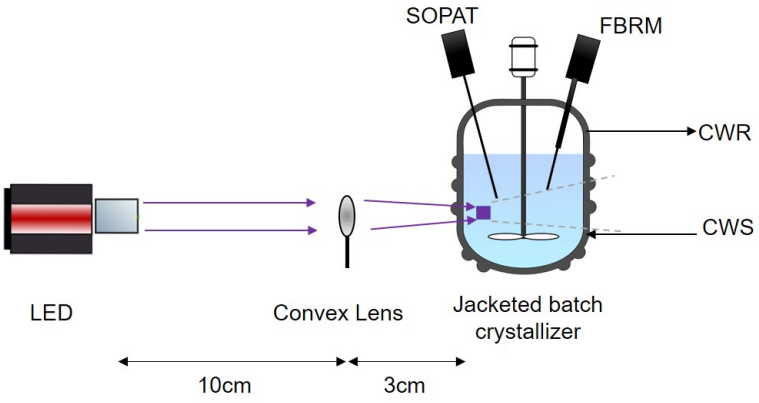

Figure A.1: The schematic for LED experiments on batch crystallizer in liter volume scale.

In this experiment, the temperature was decreased with a linear cooling rate of 0.3°C/min till the target temperature of 26°C was reached (see Figure 4.5). LED light was turned on at 26°C and remain on till the crystals were observed in the bulk solution. The maximum power measured by powermeter at a distance of 3cm after the lens, was 6 W and the area of beam spot was 1 cm^2. Hence, a maximum intensity of 6 W/cm^2 was achieved. However, the actual intensity can be higher due to curved surface of crystallizer wall.

A.3. RESULTS AND DISCUSSIONS

These experiments were performed using a supersaturation of 1.0027 because the induction time of control experiment is maximum at SS = 1.0027 as compared to other supersaturation, thus the solution is quite stable. The measurement of induction time for supersaturation of 1.0027 at 26°C was done for multiple runs of LED experiments. Figure A.2 represents the induction time for four experiments conducted.

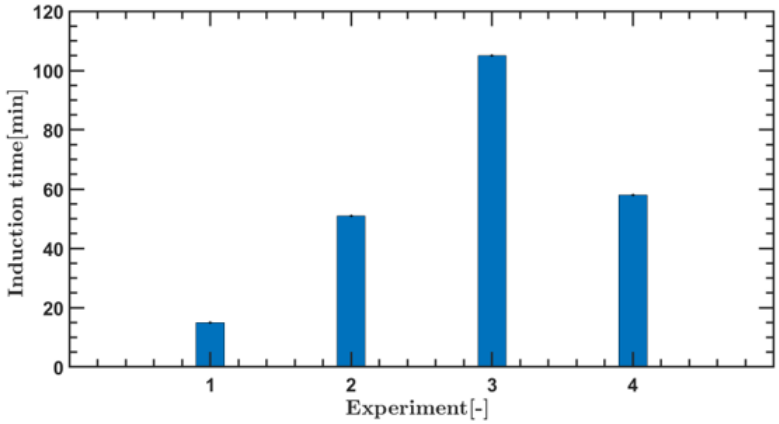

Figure A.2: The induction time measurement in led experiment.

It can be noted that the induction time variation in this experiment lies in between the induction time of the control experiment as mentioned in Figure 4.7. At this stage, it is very inconclusive to say if the nucleation is due to LED or due to spontaneous nucleation under cooling. Moreover, the intensity achieved by this LED source is 6 W/cm^2 that is $\mathcal{O}(10^6)$ less than the threshold intensity (MW/cm^2) mentioned for NPIN in literature[13].

The NPLIN intensity can be achieved by collimating the beam and converging tightly by optics to a very small spot in the range of μm. But, the available LED source is the combination of four in-built individual LED sources as shown in Figure A.3. Furthermore, the shape of the beam is square shape unlike the gaussian beam of Nd:YAG laser sources. This configuration makes it very challenging to converge the beam into micron range.

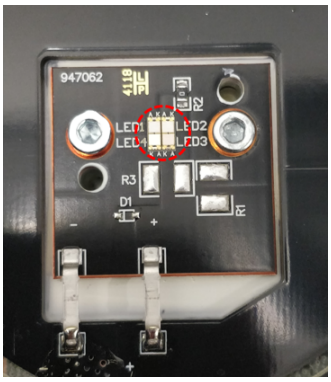

Figure A.3: The internals of LED showing the combination of four individual led.

A.4. CONCLUSION

The induction time measurement by the LED experiments gave an inconclusive result at an intensity of 6 W/cm^2. There was a limitation to increase the intensity due the internal combination of four LED sources. The use of fiber laser can provide a better alternative for existing LED with narrow beam diameter with collimated uniform beam.

BIBLIOGRAPHY

[1] H. Kramer and G. van Rosmalen, *Crystallization,* Encyclopedia of Separation Science **1**, 64 (2000).

[2] P. A. Larsen, D. B. Patience, and J. B. Rawlings, *Industrial crystallization process control,* IEEE Control Systems Magazine **26**, 70 (2006).

[3] *Efpia, the european federation of pharmaceutical industries and associations,* https://www.efpia.eu/media/412931/the-pharmaceutical-industry-in-figures-2019.pdf, accessed: 2021-03-31.

[4] A. S. Myerson, D. Erdemir, and A. Y. Lee, *Handbook of industrial crystallization* (Cambridge University Press, 2019).

[5] A. J. Alexander and P. J. Camp, *Non-photochemical laser-induced nucleation,* The Journal of chemical physics **150**, 040901 (2019).

[6] F. Schüth, P. Bussian, P. Ågren, S. Schunk, and M. Lindén, *Techniques for analyzing the early stages of crystallization reactions,* Solid state sciences **3**, 801 (2001).

[7] H.-h. Shi, Y. Xiao, S. Ferguson, X. Huang, N. Wang, and H.-x. Hao, *Progress of crystallization in microfluidic devices,* Lab on a Chip **17**, 2167 (2017).

[8] M. L. De Castro and F. Priego-Capote, *Ultrasound-assisted crystallization (sonocrystallization),* Ultrasonics sonochemistry **14**, 717 (2007).

[9] R. Kacker, M. Radoiu, and H. J. Kramer, *Novel design integrating a microwave applicator into a crystallizer for rapid temperature cycling. a direct nucleation control study,* Crystal growth & design **17**, 3766 (2017).

[10] B. Garetz, J. Aber, N. Goddard, R. Young, and A. Myerson, *Nonphotochemical, polarization-dependent, laser-induced nucleation in supersaturated aqueous urea solutions,* Physical review letters **77**, 3475 (1996).

[11] T. Hua, O. Gowayed, D. Grey-Stewart, B. A. Garetz, and R. L. Hartman, *Microfluidic laser-induced nucleation of supersaturated aqueous kcl solutions,* Crystal Growth & Design **19**, 3491 (2019).

[12] B. C. Knott, J. L. LaRue, A. M. Wodtke, M. F. Doherty, and B. Peters, *Communication: Bubbles, crystals, and laser-induced nucleation,* (2011).

[13] R. Kacker, S. Dhingra, D. Irimia, M. K. Ghatkesar, A. Stankiewicz, H. J. Kramer, and H. B. Eral, *Multiparameter investigation of laser-induced nucleation of supersaturated aqueous kcl solutions,* Crystal Growth & Design **18**, 312 (2018).

[14] D. Erdemir, A. Y. Lee, and A. S. Myerson, *Nucleation of crystals from solution: classical and two-step models,* Accounts of chemical research **42**, 621 (2009).

[15] *Lethal injection: A mixture of pancuronium bromide, sodium pentothol and potassium chloride,* http://www.chm.bris.ac.uk/webprojects2006/Macgee/Web_project_2/Web%20Project/lethal_injection.htm, accessed: 2021-04-06.

[16] J. W. Mullin, *Crystallization* (Elsevier, 2001).

[17] F. Penha, *Unpublished artwork,* (2019).

[18] N. Kubota, *A new interpretation of metastable zone widths measured for unseeded solutions,* Journal of Crystal Growth **310**, 629 (2008).

[19] J. M. Garcıa-Ruiz, *Nucleation of protein crystals,* Journal of Structural Biology **142**, 22 (2003).

[20] C. Devos, T. Van Gerven, and S. Kuhn, *A review of experimental methods for nucleation rate determination in large-volume batch and microfluidic crystallization,* Crystal Growth & Design (2021).

[21] S. D. Thakore, A. Sood, and A. K. Bansal, *Emerging role of primary heterogeneous nucleation in pharmaceutical crystallization,* Drug development research **81**, 3 (2020).

[22] S. Karthika, T. Radhakrishnan, and P. Kalaichelvi, *A review of classical and nonclassical nucleation theories,* Crystal Growth & Design **16**, 6663 (2016).

[23] S. Dhingra, *Understanding non-photochemical laser induced nucleation,* Master thesis (2018).

[24] J. P. Kardum, A. Sander, and A. Glasnoviæ, *Batch crystallization of kcl: The influence of the cooling and mixing rate on the granulometric properties of obtained crystals,* Chemical and biochemical engineering quarterly **19**, 39 (2005).

[25] J. Mullin, M. Chakraborty, and K. Mehta, *Nucleation and growth of ammonium sulphate crystals from aqueous solution,* Journal of Applied Chemistry **20**, 367 (1970).

[26] T. Melia and W. Moffitt, *Secondary nucleation from aqueous solution,* Industrial & Engineering Chemistry Fundamentals **3**, 313 (1964).

[27] H. A. Mohameed, B. Abu-Jdayil, and M. Al Khateeb, *Effect of cooling rate on unseeded batch crystallization of kcl,* Chemical Engineering and Processing: Process Intensification **41**, 297 (2002).

[28] H. Mohameed, N. Abdel-Jabbar, K. Takrouri, and A. Nasr, *Model-based optimal cooling strategy for batch crystallization processes,* Chemical Engineering Research and Design **81**, 578 (2003).

[29] T. T. Nguyen, A. Khan, L. M. Bruce, C. Forbes, R. L. O'Leary, and C. J. Price, *The effect of ultrasound on the crystallisation of paracetamol in the presence of structurally similar impurities,* Crystals **7**, 294 (2017).

[30] J. Zaccaro, J. Matic, A. S. Myerson, and B. A. Garetz, *Nonphotochemical, laser-induced nucleation of supersaturated aqueous glycine produces unexpected γ-polymorph,* Crystal Growth & Design **1**, 5 (2001).

[31] X. Sun, B. A. Garetz, and A. S. Myerson, *Polarization switching of crystal structure in the nonphotochemical laser-induced nucleation of supersaturated aqueous l-histidine,* Crystal Growth and Design **8**, 1720 (2008).

[32] I. S. Lee, J. M. Evans, D. Erdemir, A. Y. Lee, B. A. Garetz, and A. S. Myerson, *Nonphotochemical laser induced nucleation of hen egg white lysozyme crystals,* Crystal Growth and Design **8**, 4255 (2008).

[33] A. J. Alexander and P. J. Camp, *Single pulse, single crystal laser-induced nucleation of potassium chloride,* Crystal Growth and Design **9**, 958 (2009).

[34] W. Li, A. Ikni, P. Scouflaire, X. Shi, N. El Hassan, P. Gemeiner, J.-M. Gillet, and A. Spasojevic-de Bire, *Nonphotochemical laser-induced nucleation of sulfathiazole in a water/ethanol mixture,* Crystal Growth & Design **16**, 2514 (2016).

[35] M. Nardone and V. G. Karpov, *A phenomenological theory of nonphotochemical laser induced nucleation,* Physical Chemistry Chemical Physics **14**, 13601 (2012).

[36] T. Waas, *The mechanisms of non-photohchemical laser-indusced nucleation,* Bachelor thesis (2019).

[37] X. Sun, B. A. Garetz, and A. S. Myerson, *Supersaturation and polarization dependence of polymorph control in the nonphotochemical laser-induced nucleation (nplin) of aqueous glycine solutions,* Crystal growth & design **6**, 684 (2006).

[38] Y. Liu, M. R. Ward, and A. J. Alexander, *Polarization independence of laser-induced nucleation in supersaturated aqueous urea solutions,* Physical Chemistry Chemical Physics **19**, 3464 (2017).

[39] B. C. Knott, M. F. Doherty, and B. Peters, *A simulation test of the optical kerr mechanism for laser-induced nucleation,* The Journal of chemical physics **134**, 154501 (2011).

[40] M. R. Ward and A. J. Alexander, *Nonphotochemical laser-induced nucleation of potassium halides: Effects of wavelength and temperature,* Crystal growth & design **12**, 4554 (2012).

[41] M. R. Ward, A. M. Mackenzie, and A. J. Alexander, *Role of impurity nanoparticles in laser-induced nucleation of ammonium chloride,* Crystal Growth & Design **16**, 6790 (2016).

[42] A. Siems, S. A. Weber, J. Boneberg, and A. Plech, *Thermodynamics of nanosecond nanobubble formation at laser-excited metal nanoparticles,* New Journal of Physics **13**, 043018 (2011).

[43] K. McEwan and P. A. Madden, *Transient grating effects in absorbing colloidal suspensions,* The Journal of chemical physics **97**, 8748 (1992).

[44] J. Matic, X. Sun, B. A. Garetz, and A. S. Myerson, *Intensity, wavelength, and polarization dependence of nonphotochemical laser-induced nucleation in supersaturated aqueous urea solutions,* Crystal growth & design **5**, 1565 (2005).

[45] D. Irimia, J. Jose Shirley, A. S. Garg, D. P. Nijland, A. E. van der Heijden, H. J. Kramer, and H. B. Eral, *Influence of laser parameters and experimental conditions on nonphotochemical laser-induced nucleation of glycine polymorphs,* Crystal Growth & Design (2020).

[46] M. R. Ward, I. Ballingall, M. L. Costen, K. G. McKendrick, and A. J. Alexander, *Nanosecond pulse width dependence of nonphotochemical laser-induced nucleation of potassium chloride,* Chemical Physics Letters **481**, 25 (2009).

[47] P. Barrett and B. Glennon, *Characterizing the metastable zone width and solubility curve using lasentec fbrm and pvm,* Chemical Engineering Research and Design **80**, 799 (2002).

[48] R. Shearman and A. W. Menzies, *The solubilities of potassium chloride in deuterium water and in ordinary water from 0 to 180,* Journal of the American Chemical Society **59**, 185 (1937).

[49] R. Fernandez-Prini, *Le chatelier's principle and the prediction of the effect of temperature on solubilities,* Journal of Chemical Education **59**, 550 (1982).

[50] R. Davey and J. Garside, *From molecules to crystallizers* (Oxford University Press, 2000).

[51] S. A. Kulkarni, S. S. Kadam, H. Meekes, A. I. Stankiewicz, and J. H. ter Horst, *Crystal nucleation kinetics from induction times and metastable zone widths,* Crystal growth & design **13**, 2435 (2013).

[52] *Technical guide, in-process particle characterization of suspensions and emulsions,* https://www.mt.com/dam/LabDiv/Campaigns/chem/Downloads/Control.pdf, accessed: 2021-03-07.

[53] T. Leyssens, C. Baudry, and M. L. Escudero Hernandez, *Optimization of a crystallization by online fbrm analysis of needle-shaped crystals,* Organic Process Research & Development **15**, 413 (2011).

[54] R. Irizarry, A. Nataraj, and J. Schoell, *Cld-to-psd model to predict bimodal distributions and changes in modality and particle morphology,* Chemical Engineering Science **232**, 116332 (2021).

[55] R. Kacker, *Nucleation control: Microwave, ultrasound and laser as tools to control the number of nuclei in crystallization processes,* Doctoral thesis (2018).

[56] S. S. Kadam, S. A. Kulkarni, R. C. Ribera, A. I. Stankiewicz, J. H. ter Horst, and H. J. Kramer, *A new view on the metastable zone width during cooling crystallization,* Chemical engineering science **72**, 10 (2012).

[57] S. Jiang and J. H. ter Horst, *Crystal nucleation rates from probability distributions of induction times,* Crystal Growth & Design **11**, 256 (2011).

[58] O. Galkin and P. G. Vekilov, *Direct determination of the nucleation rates of protein crystals,* The Journal of Physical Chemistry B **103**, 10965 (1999).

[59] A. M. Fitzgerald, O. J. Barnes, I. Smart, and D. I. Wilson, *Measurement of particle size distribution of tripalmitin crystals in a model solution using a laser diffraction method,* Journal of the American Oil Chemists' Society **78**, 1013 (2001).

[60] J. Desarnaud, H. Derluyn, J. Carmeliet, D. Bonn, and N. Shahidzadeh, *Hopper growth of salt crystals,* The journal of physical chemistry letters **9**, 2961 (2018).

[61] B. L. M. Lung-Somarriba, M. Moscosa-Santillan, C. Porte, and A. Delacroix, *Effect of seeded surface area on crystal size distribution in glycine batch cooling crystallization: a seeding methodology,* Journal of crystal growth **270**, 624 (2004).

[62] J. Holaň, L. Ridvan, P. Billot, and F. Štěpánek, *Design of co-crystallization processes with regard to particle size distribution,* Chemical Engineering Science **128**, 36 (2015).

[63] O. Narducci and A. Jones, *Seeding in situ the cooling crystallization of adipic acid using ultrasound,* Crystal growth & design **12**, 1727 (2012).

[64] H. Li, Y. Kawajiri, M. A. Grover, and R. W. Rousseau, *Modeling of nucleation and growth kinetics for unseeded batch cooling crystallization,* Industrial & Engineering Chemistry Research **56**, 4060 (2017).